

Time Reversed Electromagnetic Wave Propagation as a Novel Method of Wireless Power Transfer

by

Gemstone Team TESLA

Frank Cangialosi, Anu Challa, Tim Furman, Tyler Grover, Patrick Healey, Ben Phillip, Scott Roman, Andrew Simon, Alex Tabatabai,
Liangcheng Tao

Professor Steven Anlage, Mentor

Thesis submitted in partial fulfillment of the requirements of the
Gemstone Program, University of Maryland, College Park, 2016

Committee

Steven Anlage
Romel Del Rosario Gomez
Raymond John Sedwick
Biniyam Taddese
Vladimir Talanov

Time Reversed Electromagnetic Wave Propagation as a Novel Method of Wireless Power Transfer

by

Gemstone Team TESLA

Submitted to the Gemstone Program, University of Maryland, College Park
on April 15, 2016, in partial fulfillment of the
requirements of the Gemstone Program, University of Maryland, College Park, 2016

Abstract

We investigate the application of time-reversed electromagnetic wave propagation to transmit energy to a moving target in a reverberant environment. “Time reversal” is a signal focusing method that exploits the time reversal invariance of the lossless wave equation to direct signals onto a single point inside a complex scattering environment. In this work, we explore the properties of time-reversed microwave pulses in a low-loss ray-chaotic chamber. We measure the spatial profile of the collapsing wavefront around the target antenna, and demonstrate that time reversal can be used to transfer energy to a receiver in motion. We discuss the results of these experiments, and explore their implications for a novel wireless power transmission system.

Thesis Supervisor: Steven Anlage

Title: Professor

Acknowledgments

Team TESLA would like to thank Nevenka Zdravkovska, the Gemstone Staff, and the graduate students of Dr. Anlage's lab for all of the help they have given the over the years

In particular we would like to thank Dr. Anlage, Bo Xiao, and Rahul Gogna. Their guidance, patience, and support were critical to all of our successes. We learned so much from all of you.

Contents

1	Introduction	1
2	Literature Review	5
2.1	Wireless Power Transfer Vocabulary	6
2.1.1	Efficiency	7
2.1.2	Range	8
2.1.3	Maximum Power	8
2.1.4	Active or Passive Transmission	8
2.1.5	Size and Weight of Transmitting and Receiving Units	9
2.1.6	Health Concerns	9
2.2	Overview of WPT Technologies by Company	10
2.2.1	Very Short Range	10
2.2.2	Medium Range	11
2.2.3	Long Range	15
2.3	Time Reversal	18
2.3.1	Conceptual Overview of Time Reversal	18
2.3.2	History of Time Reversal Research	20
2.4	Experimental Work	24
3	Methodology for Conducting Linear Time Reversal Measurements	25
4	Overlapping Reconstructions	29
4.1	Purpose	29
4.2	Methodology	30
4.3	Results	31
4.4	Discussion	32
5	Spatial Profiling	35
5.1	Purpose	35
5.2	Methodology	36
5.3	Results	37
5.4	Discussion	38
6	Moving Reconstructions	41

7 Methodology for Conducting Nonlinear Time Reversal Measurements	45
8 Using Nonlinear Time Reversal for Selective Reconstructions	49
8.1 Purpose	49
8.2 Methodology	50
8.3 Results	52
8.4 Discussion	53
9 Numerical Simulations of the Nonlinear Time Reversal Process	55
9.1 Purpose	55
9.2 Methodology	57
9.2.1 Equipment	57
9.2.2 Time-Reversal and Nonlinear Sona Extraction	58
9.2.3 Defining and Controlling the Nonlinear Element	61
9.3 Results	63
9.3.1 Simultaneous Nonlinear Time Reversal	63
9.3.2 Discussion of Simultaneous Nonlinear Reconstructions	67
9.3.3 Simulation of Selective Collapse of NLTR	68
9.3.4 Discussion of Selective Nonlinear Time Reversal	73
9.3.5 Simulation of Transmission Efficiency of NLTR Process	74
9.4 Conclusion	76
10 Ferromagnetic Nanorods as a Nonlinear Beacon	79
10.1 Purpose	79
10.2 Methodology	79
10.3 Results	82
10.4 Discussion	83
11 Development of a Super Rectenna	85
11.1 Goals of Rectenna	85
11.2 Diode Selection and Testing	86
11.3 Antenna Design	88
11.4 Rectenna Testing	90
11.4.1 DC Power Characterization	90
11.4.2 Harmonic Generation	95
11.5 Discussion	96
12 Conclusion	99
12.0.1 Equipment and Expertise Limitations	99
12.0.2 Future Work and Considerations	101
Glossary	105

List of Figures

2-1	WiTricity schematic	12
2-2	The resonating chamber of a typical laser. The gain medium allows for stimulated emission of photons. The 95% reflective mirror partially transmits light, which is observed as the output of the laser [35].	16
2-3	A modification of the traditional laser resonating cavity to allow for collimation and coherency of the stimulated photons [35].	16
2-4	The setup of the Wi-Charge system. The fully reflective mirror is on the transmitter, while the 95% reflective mirror is located within the receiver device. Behind the receiver's mirror is a photovoltaic cell to convert the light back into an electrical signal to power a battery [35].	16
2-5	Recorded sona and reconstruction from a typical TRM experiment . .	19
3-1	Lab equipment setup	26
3-2	Conceptual overview of linear time reversal	28
4-1	Overlapping sonas	31
4-2	Overlapping reconstructions	32
4-3	Max V _{pp} from overlapping reconstructions	33
5-1	Spatial profile of peak-to-peak voltage amplitudes of reconstructions investigated at carrier frequencies ranging from 4 to 9 GHz in 1 GHz steps. The inset shows the inverse of the fit b values versus carrier frequency, showing the expected linear relationship.	37
5-2	Measured peak-to-peak voltage amplitude of reconstructions received in the vicinity of a time-reversed wave collapse location with a 5 GHz carrier frequency, and fit to the $\text{sinc}(x)$ function.	38
6-1	Voltage measured during moving reconstructions	43
7-1	Conceptual overview of nonlinear time reversal	47
8-1	Selective Targeting Setup	51
8-2	Selective Targeting Linear Port	52
8-3	Selective Targeting Nonlinear Port	52
9-1	Example of inverted and non-inverted interrogation signals	59
9-2	Demonstration of pulse inversion	60

9-3	CST circuit model of a diode	62
9-4	I-V curves of diodes with different voltage knees	63
9-5	The Cut Box Model	65
9-6	S_{11} spectrum of the Cut Box Model	66
9-7	Simultaneous reconstructions on two diodes	67
9-8	Nonlinear response due to different diode settings	70
9-9	Selective reconstruction on a V_k^{low} diode	71
9-10	Selective reconstruction on a V_k^{high} diode	72
9-11	Example transfer efficiency for a two-diode simultaneous reconstruction	75
9-12	Geometry of the Room Model	76
10-1	Initial ferromagnetic nanorod experimental setup	80
10-2	Antenna used with ferromagnetic nanorods in the Gigabox	81
10-3	Ferromagnetic nanorod experimental results	82
11-1	Rectenna design	89
11-3	Rectified DC power	92
11-5	Rectification efficiency	95
11-6	Experimental setup for harmonic generation testing.	96

List of Tables

2.1 Comparison of wireless technology companies and their products' capabilities	6
9.1 Computer specifications	58
11.1 Datasheet for diode used in rectenna construction	88

Chapter 1

Introduction

In 1998, accessing the Internet required a clunky desktop computer and a dial-up subscription. When Apple integrated WiFi into its iBook computers under the brand name “AirPort” the following year, it forced other industry giants to compete and revolutionized wireless networking [2]. If not for the adoption of this technology along with the advent of wireless data-enabled and commercially available cell phones such as Nokia’s Communicator 9000 [1], cell phones would never have evolved to surpass their primary function as telephones and become the communication necessity they are today.

The ubiquity of WiFi and wireless communication revolutionized the way society interacts with the Internet. Suddenly, portable devices became powerful standalone devices rather than accessories to their desk-bound counterparts. Cell phones rivaled computers in necessity and ubiquity, and eclipsed their predecessors in terms of productivity. Coffee shops, airports, and hotels transformed from physical meeting places to universal hotspots, enabling the masses to bridge distances, connect instantly, and

effectively trivialize time and space quite literally in the palms of their hands. This is the power of wireless technology.

So then, why does society continue to labor under the burden of wires? Having enjoyed rewards of another relatively nascent wireless technology, why do we hesitate to cut the cord?

Wireless power transfer (WPT)-enabled mobile devices have the potential to be a disruptive technology on the consumer technology market. Investments in WPT have grown dramatically in the past decade, and more technologies have started integrating WPT into their systems at the consumer level.

The result is a growing number of WPT methods seeing practical application. These techniques can successfully power and charge a wide range of consumer products, from cell phones to cars. However, they still face significant disadvantages in transmission distance and efficiency. Most require line of sight to operate.

Gemstone Team TESLA proposes time-reversed electromagnetic wave propagation (to be abbreviated “time-reversal” or “TR” in this document) as a novel WPT method. In particular, TR’s ability to maintain connection even when line of sight is lost opens up a new range of possible applications. To support this proposal, the team has performed a number of exploratory experiments on the topic of TR applied to WPT. These experiments are concerned primarily with understanding the fundamental engineering realities that would be necessary to build a working TR WPT system.

In this paper, TESLA overviews the state of the art of both consumer wireless power transfer technologies and time reversal. Major innovations are outlined, as

are current limitations. The team's experiments are then detailed individually. The purpose, methodology, and results for each experiment are explained. The results of each experiment and their significance are then discussed in the context of TR WPT. The results of the team as a whole are discussed in a similar way. Finally, the team makes suggestions for future research that could be made in this field, for the benefit of future researchers.

Chapter 2

Literature Review

Commercial wireless power transfer technologies have developed as a response to both the ubiquity of mobile devices and limitations in traditional wired power. These technologies differ in range, efficacy, and method, but suggest an overall attempt to shift away from traditional charging mechanisms. This literature review will focus on the distinct methods that make up the current state-of-the-art of wireless power. These methods and companies are not meant to be exhaustive, but should be recognized as a bird's-eye-view toward these liminal technologies. This review will additionally explore WPT technologies based on their applicable ranges.

At the conclusion of this state-of-the-art overview, we will discuss both the general operation of time reversal and the historical developments of the TR field. This will include the acoustical roots of TR by Claire Prada and Matthias Fink, later communication accomplishments by Steven Anlage, and TESLA's modern WPT application.

Company	Method of Power Transfer	Max Power Delivered (W)	Approx. Range (ft.)
Cota	Concentrated Microwaves	1	30
Powermat	Inductive Coupling	5 to 50	Touching
uBeam	Ultrasound	Unknown (minimum 1.5)	3 to 13
WattUp	RF	10	15
Wi-Charge	Laser	10	30
WiTricity	Inductive Coupling	Scalable, on the order of 1000	7

Table 2.1: Comparison chart of wireless technology companies and their products' capabilities¹

2.1 Wireless Power Transfer Vocabulary

Several groups have already made practical WPT technologies. In this paper Powermat, WiTricity, Wattup, uBeam, Cota, and Wicharge will be considered as the state of the art WPT methods. The technologies these companies use in their products will be compared using several different metrics, defined here. The capabilities of these technologies under these metrics are summarized in Table 2.1, and discussed in detail in the following sections. These companies represent many of the major players in the current WPT industry that either currently have a product on the market, are in the process of commericalizing a product, or have plans to commercialize a produce in the next few years.

¹Some companies are still in their early stages and thus have not released full details about their technology yet. The information in this table reflects publicly disclosed information at the time of writing.

As can be seen, the different WPT technologies vary wildly in both their methods of operation and their intended application. Comparing different WPT technologies is difficult because the measures of characterizing performance used in Table 2.1 are poorly defined. The field of WPT lacks one central governing body that defines such performance metrics. This, combined with the constant battle for market prominence leads to many crucial details being withheld due to Intellectual Property (IP) rights. Due to these complications, we will specify our own definitions of performance metrics important to this thesis.

2.1.1 Efficiency

Efficiency in particular is difficult to quantify, as there does not currently exist a standardized definition used by all parties. In the literature, efficiency of transfer has included:

- the amount of energy delivered to the target compared to the amount of power drawn by the transmitter
- the transfer between antennas within a setup, with other losses (such as those due to rectifiers after transmission) being ignored

Here, the team defines efficiency as the amount of power delivered to the battery of the target device compared to the amount of electrical power input into the transmitter.

2.1.2 Range

Range is defined here as the maximum distance that a given amount of power can be transmitted. Due to the restrictive nature of IP for the discussed companies, this definition may be generalized to the distance that a company claims in their press materials.

2.1.3 Maximum Power

The maximum amount of power that can be transmitted to a target using a given technology. Typically, this value is cited at relatively short distances, much shorter than the previously stated range. It should be specifically noted that there is generally a tradeoff between maximum power and range that is unavoidable.

Maximum power limits the devices that can be powered by a given technology. While high power transmission is not important for all devices, a larger range of power improves the flexibility of the technology.

2.1.4 Active or Passive Transmission

Some technologies require the device being powered to actively participate in the powering process, usually by broadcasting a signal to the WPT transmitter. We call this active transmission. Others, like charging mats, are “always on” as long as the device to be powered is within range: from the device’s point of view, this is passive transmission.

2.1.5 Size and Weight of Transmitting and Receiving Units

With the use of WPT technologies, the viability of the technologies towards particular applications needs to be examined. Some example criteria for examining this viability are size and weight constraints of the application. These criteria are emphasized in the application of WPT for mobile devices, where WPT technologies with smaller and lighter receivers are better suited.

2.1.6 Health Concerns

Electromagnetic radiation is known to have potentially harmful effects to biological tissue at sufficiently large energy density levels [3]. The benchmark that is used to measure the applied energy density that is transmitted to a person's skin is referred to as Specific Absorption Rating (SAR), which is a measure of the energy deposited per unit mass of a material. In this case, the material is skin tissue and the SAR value is averaged over the entire body to arrive at a final value. In the US, the FCC legal limit on SAR is 1.6 W/kg [25]. As a reference, the iPhone 5 has a cited SAR value of 1.18 W/kg [25]. It is generally accepted that cell phone use is safe. As long as our TR process does not exceed the 1.6 W/kg value, then we may assume it will be safe for human use and we do not need to be concerned with biological harm, as the FCC deems this a safe level of electromagnetic radiation.

2.2 Overview of WPT Technologies by Company

In order to classify the different companies, the most simplistic manner is to do so based on our definition of range. For the purposes of this discussion, we note 3 ranges: (1) very short range (<1 foot), (2) medium range (max of 15 feet), and (3) long range (max of 30 feet). Now that we have defined a basic classification system for the current WPT technologies we may proceed to a more in-depth discussion of the companies themselves.

2.2.1 Very Short Range

Powermat

The most restrictive technology in terms of range is that of Powermat. Devices are charged by being placed on the charging mat. Harnessing inductive coupling, the same method used to charge electric toothbrushes, Powermat has virtually no charging range, as the device and the charger must be in full contact. The technology is capable of charging multiple devices, but the system requires compatibility devices for any that are not already Powermat-enabled off-the-shelf.

As the charging mat is wired, its range is still restricted to the length of a power cord. If the device is not compliant with the Powermat standard, then it must be plugged into a compatibility device anyway. That said, the mat can deliver between 5 and 50W, making it a very effective charging tool. Powermat compatible devices can be made without any external plugs, which could be desirable for applications such as waterproofing. Another interesting application has been the implementation

of PowerMat devices inside furnature[9]. This allows tabletops to be transformed into charging surfaces.

2.2.2 Medium Range

WiTricity

Boston-based company WiTricity has expanded the previously discussed magnetic induction using a method they call highly resonant magnetic coupling (HRMC). Whereas traditional magnetic induction operates on the order of centimeters, HRMC is applicable at the meter scale. WiTricity reports 50% efficiency at two meters, followed by 10% efficiency at four meters [19, 32]. HRMC have charged multiple devices without seemingly sacrificing overall efficiency [19]. The public demonstrations by WiTricity show that HRMC can transmit power ranging from milliwatts to kilowatts, significantly more than was practical with traditional induction [19].

HRMC uses magnetic induction to transmit energy between two coupled antennas. HRMC continually adjusts the coupling of transmitter and receiver antennas to keep both at a mutual resonant frequency. This technique, impedance matching, minimizes the amount of wave reflection inside the transmitter and receiver circuits, maximizing the energy passed to the load component. This process requires a continuous proprietary feedback mechanism to optimize the receiver for the given distance from the transmitter.

WiTricity has demonstrated that the range of HRMC can be increased through the use of coupled relays. These relays can be coupled with the transmitter, allowing

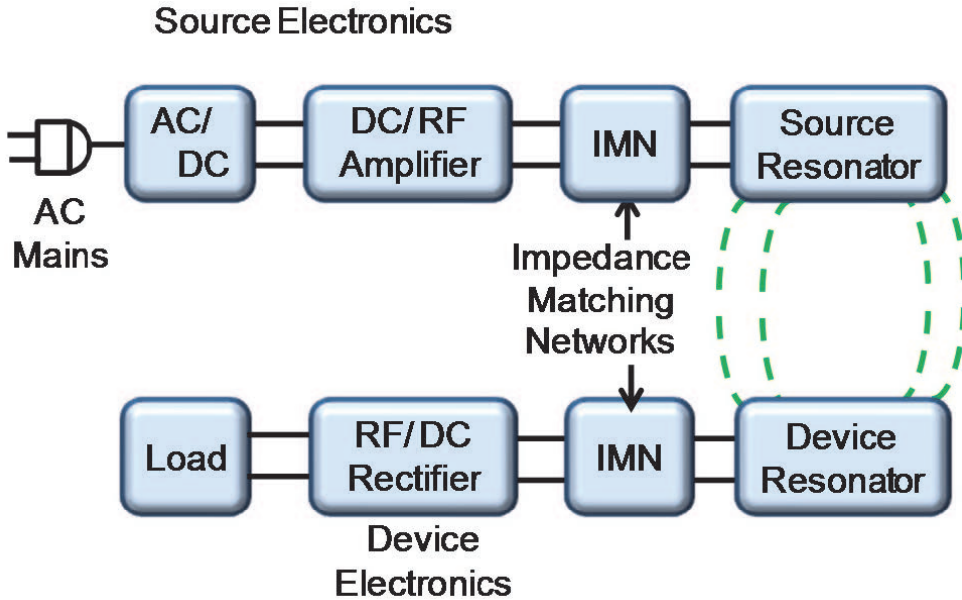


Figure 2-1: Schematic of WiTricity’s HRMC System [19]

the effective range of the transmitter to increase with minimal additional loss [7].

WattUp

Our next mid-range WPT company is named WattUp. The central idea of this company’s method is to use bluetooth to transfer RF signals containing information about the receiver’s location relative to the transmitter so that the transmitter may focus energy on the receiver [11]. Once it has locked in a signal, it may boost the output power from mW RF signals to multiple W RF signals such that the receiver can charge. WattUp highlights two main features to its technology: (1) the range over which 1–4 W may be quickly and safely transmitted and (2) the relatively large number of devices that may be powered at once (currently 12, with 24 being available in the future) [11].

WattUp cites that they may deliver up to 4 W to 4 devices simultaneously within

0-5 feet of the transmitter, 2W to 4 devices simultaneously within 5–10 feet, and 1 W within 10–15 feet [11]. This inverse relationship between delivered power and range is similar to the trend seen with WiTricity, as previously discussed. These numbers only represent the current model and demonstration version of the technology. WattUp claims that for ranges <5 feet, the device will charge as if it were plugged into a wall outlet, for 5-10 feet, the device will resemble USB port charging from a computer, and for 10–15 feet users can still power up at slower charge rates. Based on the aforementioned values provided by WattUp, the overall max range is $\tilde{15}$ feet with a max output power of $\tilde{10}$ W, although these two conditions may not be met at the same time.

The technology itself uses two separate RF frequencies to perform wireless charging, representing both the Bluetooth communication (2.4 GHz) and power transfer frequency (5.7 GHz) [11]. Both of these frequencies are allowed unlicensed frequency bands that are known to be used for wireless communication. We believe that WattUp chose to use separate frequencies in order to more easily differentiate the signals used for either targeting or power transfer. As the targeting algorithm is proprietary, we are unable to comment on their exact methodology for targeting the receiver.

uBeam

The final primary medium range WPT titled uBeam uses an entirely unique method compared to other companies/methods, relying on ultrasonic waves rather than electromagnetic waves [10]. One can imagine their system as an extremely high power microphone and speaker combination that specifically sends the sound to a device

location. Although uBeam is unique in its approach, it boasts comparable range and power levels when discussed next to other WPT companies.

The first difficulty to using sound waves as opposed to electromagnetic waves is the inherent dissipative nature of air as a medium. Due to this characteristic, uBeam uses output sound levels of 145–155 dB ($316 - 3000 \frac{W}{m^2}$), comparable to the sound produced by a jet engine or shotgun blast [5]. In order for this level of sound to be used safely, uBeam transmission frequencies of 45–75 kHz, as this is far above the audible range of both humans and animals. As an extra safety measure, uBeam cites that “if a person were to be exposed to the uBeam ultrasound source, 99.9% of the emitted ultrasound will bounce off the skin” [10]. These considerations have allowed uBeam to stay well within the FDA safety regulations. uBeam uses a phased array transmitter with thousands of antennas that result in a power range of 1–4 m. Although the tracking and targeting algorithm is proprietary in nature, uBeam claims the ability to maintain power transfer while the receiver is moving, although uBeam does not cite specific speeds. The technology requires few obstructions in order to work due to the nature of sound as a mechanical oscillation. For example, if a cell phone is in a user’s pocket, then it will not be able to be powered as the user’s clothing will block or extremely dampen the ultrasonic waves.

As their product has not yet hit the market, numbers for uBeam’s efficiency are not available. We do know that the power output from the transmitter is 145–155 dB [10], while a reasonable output at the receiver is on the order of 1–10 watts. Based on this, the technique seems unlikely to have a high wall-to-load efficiency.

2.2.3 Long Range

Cota

Cota uses concentrated microwaves to create “pockets of energy” at precise locations.

The power-seeking device sends out pulses regularly, which, when picked up by a Cota system, trigger the system to send out a high energy pulse targeted specifically to the device’s location.

The Cota system consists of two parts: a charger and a receiver. The Cota receivers built into devices and batteries regularly send out omnidirectional beacon signals. Once the Cota charger receives these beacons, it returns thousands of targeted signals that build hotspots of energy at only the precise locations of the beacons’ locations. The charger uses 20,000 antennas to determine the exact direction the signal came from. This pinpoint precision targeting of energy safely and efficiently powers all Cota-equipped devices and batteries within its effective radius, even as they move around the room.

The technology has achieved a 30 ft range and a max power delivery of about 1 W, offering a comfortable operating radius and charging speed at about one-third the charging time via regular USB cable. It also cites the capability to charge as many devices as desired. It does use Bluetooth to link the charger to the receiver(s), which requires that the power-seeking device constantly pulse to request power. This means that charging the device is contingent on the device already having enough power to send that request.

Wi-Charge



Figure 2-2: The resonating chamber of a typical laser. The gain medium allows for stimulated emission of photons. The 95% reflective mirror partially transmits light, which is observed as the output of the laser [35].



Figure 2-3: A modification of the traditional laser resonating cavity to allow for collimation and coherency of the stimulated photons [35].



Figure 2-4: The setup of the Wi-Charge system. The fully reflective mirror is on the transmitter, while the 95% reflective mirror is located within the receiver device. Behind the receiver's mirror is a photovoltaic cell to convert the light back into an electrical signal to power a battery [35].

Also capable of a 30 ft operating radius, Wi-Charge uses a combination of a laser cavity and a photovoltaic cell to create robust power transfer systems [35]. To understand the system, it is necessary to discuss how a laser works. Consider Figure 2-

2, which depicts two mirrors and an amplifier between them. Simply put, one photon, an energetic light particle, enters the amplifier and two come out. When the photons hit the mirror, they bounce back through amplifier in the opposite direction and two photons become four. This process repeats with each ricochet against a mirror, and the energy amplifies within the system. This process of recirculating light in a positive feedback loop with an amplifier creates a resonator.

When that resonator has one mirror that is very slightly transparent, as in Figure 2-2, then a focused, high powered beam is generated. This is a laser beam.

Any particles that do not travel along the axis between the two mirrors will hit the mirror at an odd angle and bounce out of the resonator. This is why only the photons that are traveling in the direction of the axis between the two mirrors will continue to amplify.

Wi-Charge took this traditional definition of a laser, and made a few clever modifications to better suit their purposes, shown in Figure 2-3 [35].

First, they kept the components—two mirrors with an amplifier between them—but modified their arrangement. Second, they made the mirrors retro-reflectors which, unlike regular mirrors, reflect light back to their sources. The result is that the two mirrors spontaneously form a resonator when placed within each other's line of sight, although the resonator is stalled immediately when the line of sight is broken. This last property may actually be desireable in a consumer setting, as it helps to prevent energy from accumulating anywhere but the intended receiver.

In Wi-Charge's setup, one mirror and the amplifier are grouped together as the transmitter, and a second mirror and a photovoltaic cell are grouped together as the

receiver. This is shown in Figure 2-4. By placing the photovoltaic cell directly after the laser output location, the Wi-Charge system effectively converts the optical signal back to an electrical signal that can be used to charge a battery.

Wi-Charge is a long range wireless power solution that can deliver up to 10 W of power [35]. It can latch onto targets almost instantaneously and cease beaming equally quickly, intrinsically. It can also power multiple devices. However, the system does require line-of-sight.

2.3 Time Reversal

2.3.1 Conceptual Overview of Time Reversal

The lossless wave equation is time-reversal invariant: for any normally propagating wave taken to be a time-forward solution, there is a corresponding time-reversed solution representing that wave traveling in the opposite direction. The technique known as time reversal (TR) exploits this property of waves to focus a signal onto the point of origin of another previous signal. TR can locate objects without prior knowledge of their position or their surrounding geometry.

A system that performs TR is called a time reversal mirror (TRM), sometimes simply shortened to mirror. A TRM consists of one or more transmitters to introduce waves into a chamber and one or more receivers to record the echoes from it. The transmitters and receivers may (but do not have to be) the same device. TR is most effective in echoic chambers that allow waves to reflect off of its interior geometry and

return to the transmitters. Here we refer to such a chamber as “reverberant”.

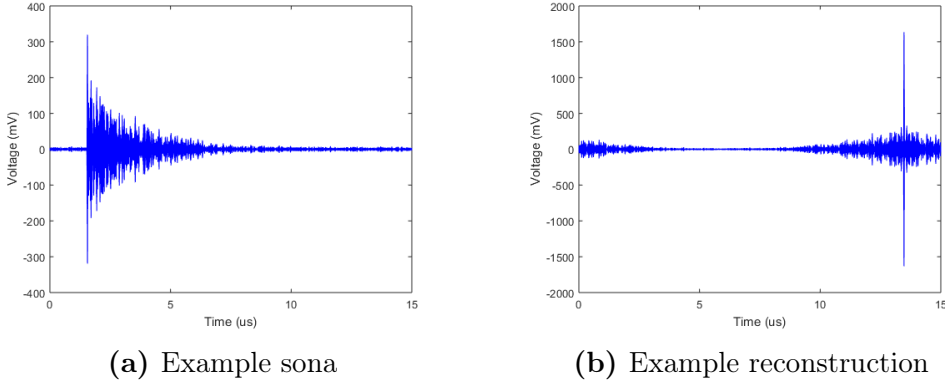


Figure 2-5: Recorded sona and reconstruction from a typical TRM experiment

A TRM works by broadcasting a waveform into the reverberant chamber and recording the resultant echo. This echo will consist of many time-shifted overlays of the original waveform. This echo will be called a “sona” in this thesis. An example sona is shown in Figure 2-5a. The sona is time reversed and rebroadcast, which will cause the waves to trace their paths in reverse and return to their source in a semi-coherent “reconstruction” of the original broadcast. An example reconstruction is shown in Figure 2-5b: in this case, the original signal was a short pulse in the same shape as the large vertical spike near the right of the figure. Since it involves waves from many scattered paths all suddenly arriving at the same point, reconstruction is also known as “collapse”.

TR is relatively versatile. If the technique is iterated exactly as described, the broadcasts will collapse more and more exactly on the strongest scatterer in the chamber [13]. Many other methods can be used to select targets more discriminately, and the generic TRM itself can be modified as well - for example, by recording directly from a target position, it is possible to create a secure channel between that point

and the transmitter [14].

2.3.2 History of Time Reversal Research

TR is a proven technique in signal processing, with applications in acoustics as well as electromagnetics. Though its publicity is limited, there is a wealth of available literature regarding TR in certain specialized areas. Here we briefly describe the development and historical applications of the technique to illustrate where TESLA’s project will expand this literature.

Time reversal as a technique was first developed in the 1990s. Some of the earliest and most influential work was conducted through teams led by Mathias Fink and Claire Prada of the University of Paris. These researchers used the technique to focus sound waves on “scatterers”, objects that reflect the pulses [23]. An array of transducers would fire a sonic pulse into some propagation medium and listen for the echo. The recording of that echo was reversed in the time domain and transmitted back into the medium. They repeated (iterated) this process, causing the acoustic signature of the strongest scatterer to appear more prominently each time. In this way, the team was able to iteratively focus on the scatterers without needing prior knowledge of their location. Prada and her team submitted this DORT (French acronym, English: Decomposition of the Time Reversal Operator) method as a process for finding cracks or faults in structural members [23]. More importantly, Prada et al. went on to demonstrate that the method could always resolve the brightest scatterer if given enough iterations, that it worked better in a heterogeneous medium than a ho-

mogenous one, and that it was both experimentally and mathematically possible to resolve multiple targets at once [24]. These discoveries generated significant interest in a subset of the acoustics research community.

Others in the field of acoustics went on to refine the DORT method as an imaging technique, and as the field gathered attention, further explored formalizing the problem in general. An excellent example of the latter is the theoretical work by D. H. Chamber in his 2007 examination of TR for target detection and characterization [8]. In 2010, Nguyen and Gan developed a way to extract much more information from an anisotropic (directionally distinct) scatterer, including its rough shape, density, and radius. In doing so, they developed a faster mathematical approach to locating their scatterers that relied on several good approximations instead of one exhaustive computation [22]. Also in 2010, Barbieri and Meo made a large contribution to the field by bringing together the DORT method, which works in linear environments, and another similar method for working in nonlinear environments. This allowed them to resolve and distinguish between linear scatterers such as holes and nonlinear scatterers such as cracks [6].

Imaging is not the only application for a focusing method, however, and others adapted the existing body of TR research to new problems. The reciprocity of the wave function that Fink and Prada relied on to develop the technique holds for all waves it can be used to model. This means that the time-reversal operation works much the same way with electromagnetic waves as it does with sound waves [8]. This was explored as early as 1999, but was largely concerned with the same imaging problems occupying those in acoustics until at least 2007 [8]. However, that gradually

began to change. In 2011, a team including graduate students from the University of Maryland posited that time reversal was an ideal mechanism for wireless communication [33]. In the same way that a sound wave could be made to collapse on a scatterer, they showed that an information packet could be made to collapse on a receiver. The team submitted this as a “green” or eco-friendly communication method, because information transfer could be accomplished using less energy [33]. Later, this same property was examined for its security benefits instead of its environmental ones. In February of 2013, a team of researchers at the University of Maryland, including Matthew Frazier and Steven Anlage, published a study discussing TR as a method to selectively send information in a chaotic wave environment [14] [30]. Essentially, the team was able to create an exclusive communication link to a certain object, without needing to know its location, and without interfering with nearby objects. In their experiment, they were able to transmit data (in the form of images) exclusively to a desired port, while the other port received only nonsense.

Beyond its practical applications, in the process, Frazier and his team used nonlinear elements to extend TR in new and exciting ways. Recall that in traditional TR many iterations are required to pinpoint the target. The addition of a significantly nonlinear element greatly simplifies the pinpointing process. When a wave strikes the element, harmonic frequencies are produced at integer multiples of the original frequency. These harmonics can be quickly located in the echo’s frequency domain and filtered to select them exclusively. The important distinction is that since the harmonics originated directly from the target antenna, all subsequent broadcasts of the TR signal will collapse on the antenna without the need for iteration [14]. Frazier

and the others put forth several exciting directions to pursue with this concept: the aforementioned secure communication channels, hyperthermic treatment of tumors, and a long range WPT system that eschews traditional high power beams. It is this last area that TESLA intends to explore.

2.4 Experimental Work

The following sections detail the research that TESLA has done in the field of TR WPT. These experiments are meant to accomplish several goals:

- Characterize the behaviors of TR relevant to WPT applications
- Understand fundamental limitations of TR applied to WPT
- Create a baseline for which future work can be done

The general methodology for the experiments is described. Then, the purpose, methodology, and results of individual experiments are discussed individually.

Chapter 3

Methodology for Conducting Linear Time Reversal Measurements

The majority of our experiments take place within an enclosed, reflective cavity called the Gigabox: an aluminum box with a metallic foil scattering paddle to make the ray trajectories more ergodic. Ray chaos ensures that a propagating pulse will eventually reach every point in the environment. This improves reconstruction fidelity. Up to five monopole antennas inject and extract electromagnetic signals from different ports in the enclosure depending on the experiment.

Our Time Reversal scheme consists of three pieces of microwave processing equipment and a desktop workstation. Interrogation pulses and time-reversed sona signals are created and broadcast using a Tektronix AWG7052 arbitrary waveform generator feeding an Agilent E8267D Vector PSG microwave source. A digital storage oscilloscope (DSO, Agilent DS091304A) is used to record waveforms of interest. MATLAB is used for signal processing and instrument control and coordination.

In many experiments, it is necessary to be able to “read” and “write” signals from the same port. Manually switching coaxial cables from the PSG to the DSO is slow and can destroy reconstructions, so we use four HP 8762C coaxial switches to reroute signals as required.

This hardware is laid out in Figure 3-1.

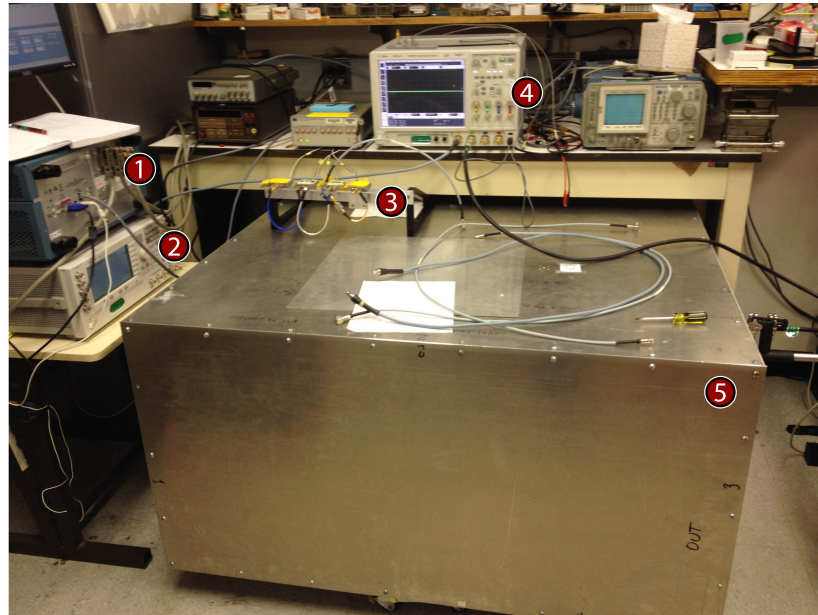


Figure 3-1: Lab equipment setup: (1) Tektronix AWG7052 Arbitrary Waveform Generator, (2) Agilent E8267D Vector PSG Microwave Source, (3) Array of four Hewlett-Packard 8762C coaxial switches, (4) Agilent DS091304A Digital Storage Oscilloscope, (5) 1.06 m^3 aluminum “Gigabox” with interior conductive scattering paddle.

Our TR experiments fall into two main categories, linear and nonlinear. Linear TR (LTR) refers to any experiment that uses a single frequency. Nonlinear TR (NLTR) makes use of harmonic reflections from the target to provide a means for isolation and targeting, a process similar to how we would envision a TR based WPT system to work. It is experimentally much simpler to create reconstructions with LTR than with NLTR, so we use it for experiments investigating the behavior of the waves rather than the behavior of the target.

This section concerns LTR experiments. Conceptually, our general process for LTR in the Gigabox is as follows: we broadcast a Gaussian interrogation pulse from one port, serving as a transmitter. This interrogation pulse reverberates and echoes around the reflective cavity. Another port, designated as the receiver, records the multipath sum of these reverberations with the oscilloscope. This summed signal is named a sona, and inherently contains information relating to the size and shape of the interrogation pulse, the location of any scattering media in the environment, and the location of both ports. That sona is reversed in the time domain and subsequently rebroadcast from the transmitting port. The signal will travel through the same multipath channels and reconstruct a time reversed version of the original interrogation pulse upon the receiver, with some additional noise. This process is illustrated in Figure 3-2.

Since this LTR process is well-suited to creating reconstructions of Gaussian waveforms, we used it for three experiments to examine characteristics and modifications of LTR itself. These were:

- Overlaying sonas to create more reconstructions closely spaced in time
- Mapping the spatial profile of a reconstruction
- Repeatedly retargeting the reconstructions upon a moving antenna

The experiments, results, and discussions for these sections are presented respectively as "Overlapping Reconstructions", "Spatial Profiling", and "Moving Reconstructions" below. The experience the team gained by performing these experiments and formulating results was invaluable in constructing and performing our later work

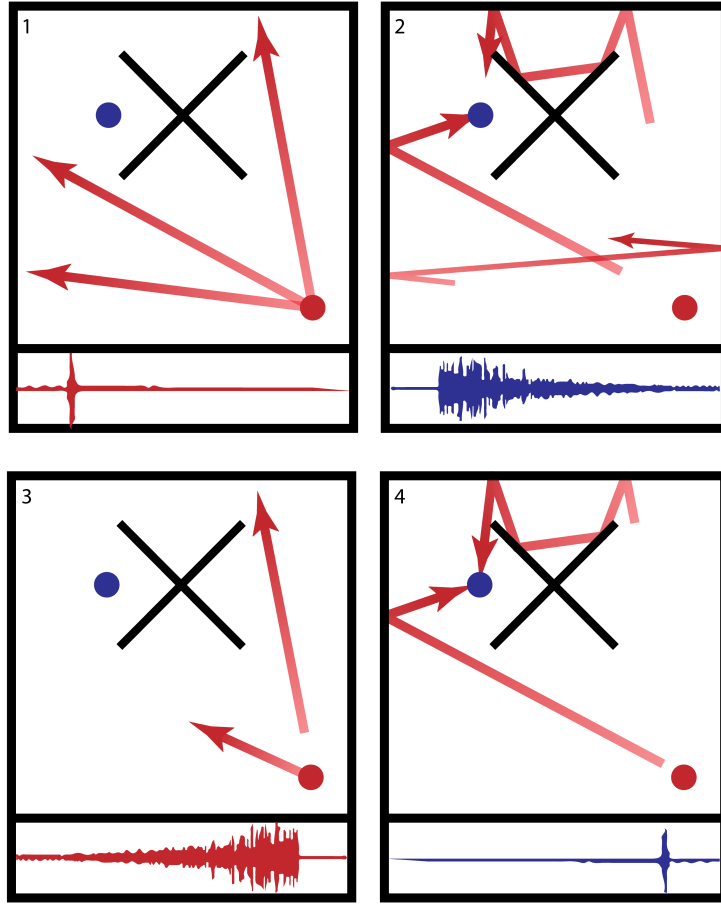


Figure 3-2: Reading order from top left: Visualization of the linear time reversal process (1) The TRM broadcasts a signal (in this case, a pulse, pictured in the inset below the panel) into the cavity, which (2) reverberates within the cavity. Some of the reflections incoherently reach the receiver as the sona, represented in blue in the inset. (3) The TRM time reverses the sona, then re-emits it into the cavity. (4) The time reversed waves coherently collapse back on the receiver in a slightly distorted reconstruction of the original pulse (inset, blue).

with Nonlinear Time Reversal (NLTR). They also demonstrate important ideas regarding the transmission of large amounts of power to the receiver.

Chapter 4

Overlapping Reconstructions

4.1 Purpose

Frazier et al. demonstrate that the sona of a given interrogation pulse is significantly longer than the pulse that generated it [14]. This stands to reason, given that the sona represents reflections of the initial pulse shifted in time by differing path lengths.

The reverse is also true: A time reversed sona will generate a reconstruction that is significantly shorter than it in time. This trait imposes a limitation on the ability of time reversal to transmit power, especially given that it is difficult to pack a large amount of energy into a short period of time. To increase the amount of energy transmitted, we desire to send reconstructions more frequently than the length of the sona will allow. However, transmitting multiple sonas at once from the same antenna is possible—copying and shifting the signal in time can allow several signals to be sent in less time than the sum of the individual sona time lengths. This will in turn result in multiple transmitted reconstructions, and improved power transmission.

A concern with the above method is whether or not it would result in lost information and consequently degraded reconstruction quality. Sonas are sinusoidal signals—if overlaid, they will interfere constructively and destructively. Destructive interference may result in the “deletion” of transmission paths, reducing the efficiency of the TR process and decreasing the fidelity of the created reconstructions. In this experiment, we are interested in understanding the degree to which superimposing sonas will degrade the ability to transmit energy between ports using linear time reversal.

4.2 Methodology

This test sought to evaluate the practicality of overlapping sonas as a method of transmitting power. This experiment was done using the basic, two-port linear time reversal scheme, described in Section ???. A sona was generated with a 3.9 GHz interrogation pulse. To verify that the sona could converge on the target, it was time reversed without any further manipulation, and injected back into the cavity. The reconstruction was recorded and compared to the original interrogation pulse to check for irregularities.

Once the efficacy of the single sona was established, the experiment was modified. Several sonas were superimposed with a constant time shift, resulting in evenly spaced copies of the verified sona across the total broadcast window. Figure 4-1 gives an example of sonas overlapping in this way. The resulting signal was then time reversed and broadcast through the linear system in the same manner as before, which resulted

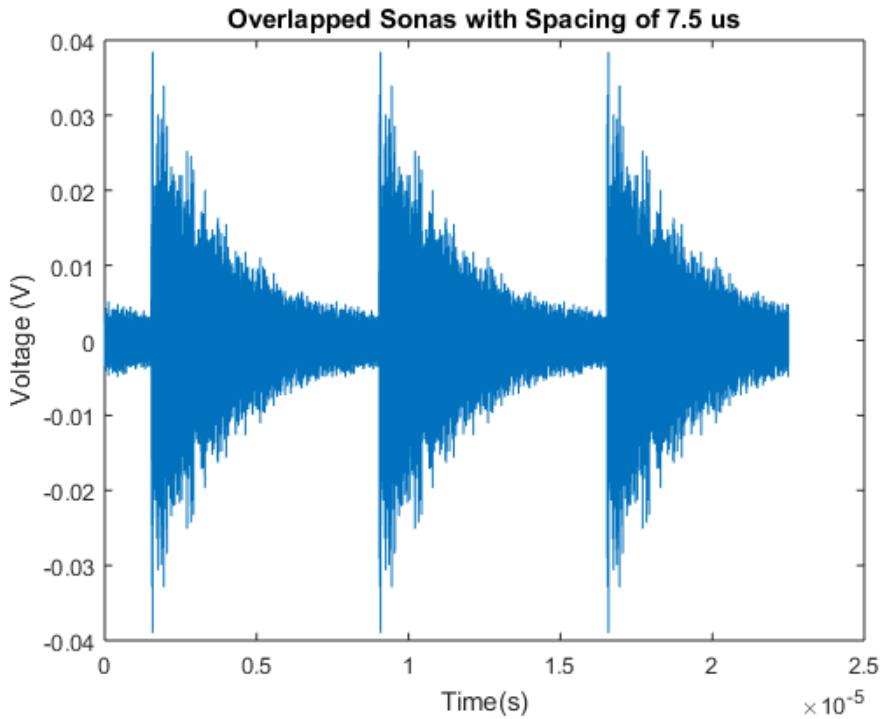


Figure 4-1: Overlapping sonas with a spacing of $7.5 \mu\text{s}$.

in the reconstructions in Figure 4-2. This test was repeated many times, with time offsets varying between $0.1 \mu\text{s}$ and $15 \mu\text{s}$, by increments of $0.1 \mu\text{s}$.

4.3 Results

For each setting of the time delay, a measure of the power received was calculated from a trapezoidal Riemann sum of the square of the recorded voltage across a recorded $15 \mu\text{s}$ window. We call this quantity the integrated power, and it is proportional to the power that is accepted at the receiver. The integrated power for each value of the repetition rate is plotted in Figure 4-3. Increasing the number of sonas should increase the amount of power transmitted in a given time frame, if the amplitude of each reconstruction remains constant. However, we actually observed an inverse

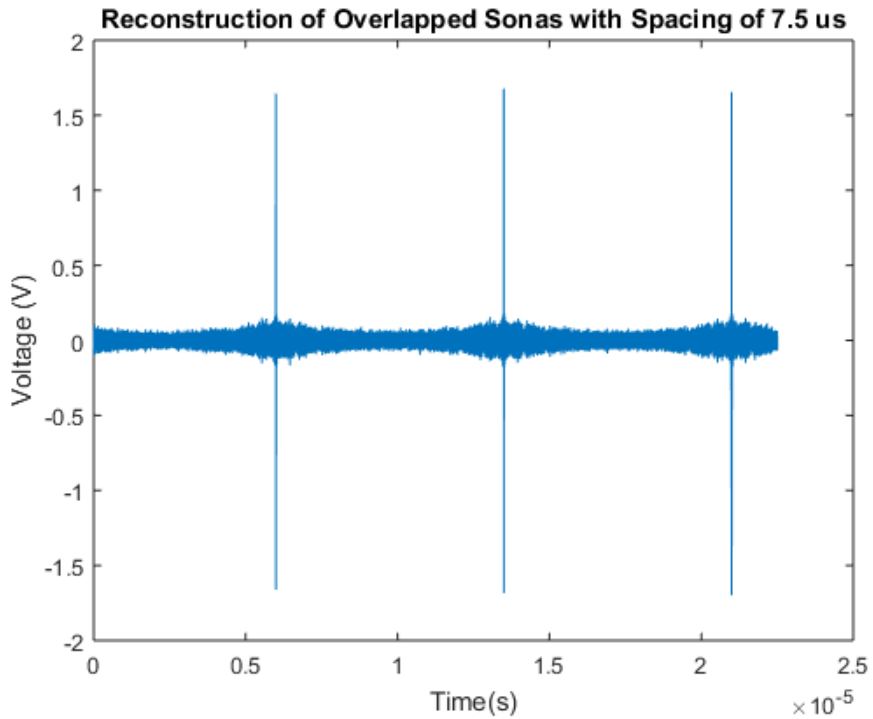


Figure 4-2: Reconstructions resulting from the sonas in 4-1.

relationship between repetition rate of the sonas and total power within the recorded reconstruction signal. The trend observed in Figure 4-3 is more complex than we had anticipated, displaying stratified bands within an exponential decay envelope.

4.4 Discussion

We hypothesized that overlapping reconstrurctions by overlaying sonas could result in more effective power transmitted per duty cycle. Our experiments seemed to support this in that the number of reconstructions in the cycle could be increased while maintaining their characteristic shape. When the integrated power was plotted against the repetition rate, we found that the power actually exhibited the opposite trend as we had expected. We believe these results to be a combination of two factors.

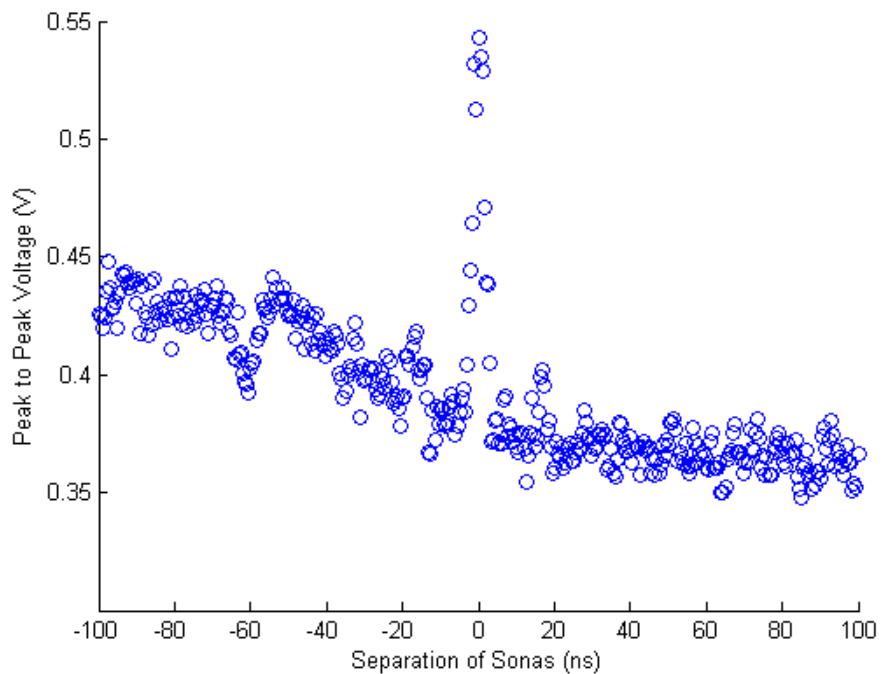


Figure 4-3: Peak to peak voltage versus number of overlapping reconstructions.

The loss of information due to destructive interference during sona superposition, and the function of power scaling within the PSG signal generator both may have contributed to these strange results. The generator attempts to level a preset amount of power across the entire broadcast window, which results in the discontinuities when mechanically switching source components throughout the sweep. However, without intimate knowledge of the PSG's inner workings, it is near impossible to extract any meaningful information regarding the origin of these bands. We recommend that future research be conducted on this phenomenon, to either confirm our results or to demonstrate that they are an artifact of our equipment limitations.

Chapter 5

Spatial Profiling

5.1 Purpose

A major concern with the practical application of TR to WPT is the ability of WPT to safely and consistently converge on its target. An ideal TR WPT system will focus large amounts of energy on a very small space. However, the question remains: how small of a space is it focused in?

The answer to this question will have major repercussions on the ability of TR to be used in a WPT context. If the area of reconstruction is large, additional energy may be directed to the area around the target. The increased energy density in this region will make losses due to absorption much higher than in other parts of the chamber. More importantly however, this absorbed energy may damage circuitry or biological matter near the TR receiver.

Clearly, the spatial profile of a reconstruction should be as small as possible. For TR WPT to be used on small electronic devices, the profile should be small enough

not to damage circuits or biological matter within a centimeter or so of the device.

An experiment was done to characterize this behavior, as it exists in our setup.

5.2 Methodology

Characterization of the spatial profile was done in the same aluminum cavity used in the linear and nonlinear time reversal tests, listed above.

The basic time reversal process in this environment proceeds as follows: First, a 50 ns Gaussian pulse (with a carrier frequency of 5 GHz) is injected into the cavity through the transmitting antenna. That sona is measured at the receiving antenna (Fig. 1b). The sona is then time reversed and injected into the transmitting antenna. The result is a reconstruction of the initial pulse back at the receiving antenna (Fig. 1c). This process makes use of another robust symmetry, namely the spatial reciprocity of the wave equation. Two monopole antennas inject and extract electromagnetic signals from different points in the enclosure. A transmitting antenna is attached to the cavity wall opposite the receiving antenna. The receiving antenna is attached to a panel that can move vertically with a total range of 70 millimeters. Motion of the receiving antenna is achieved using an externally-mounted PI MikroMove M-415.DG translation stage and the enclosure remains sealed during the translation. Interrogation pulses and time-reversed sona signals are created and broadcast using a Tektronix AWG7052 arbitrary waveform generator feeding an Agilent E8267D Vector PSG microwave source. A digital storage oscilloscope (DSO, Agilent DS091304A) is used to record waveforms of interest. MATLAB is used for signal processing and

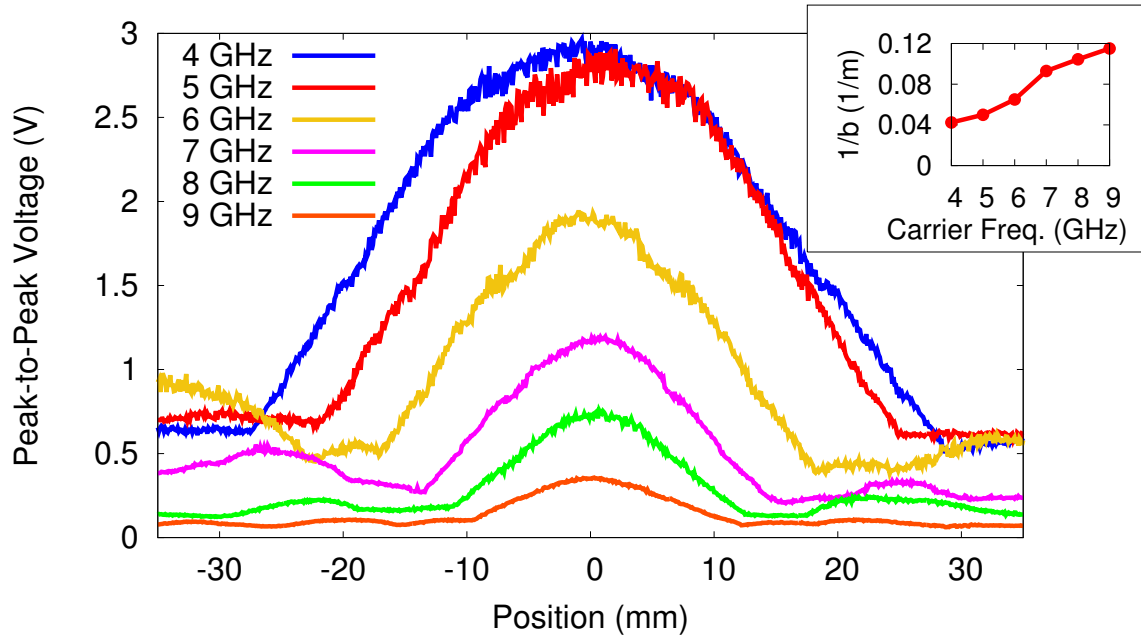


Figure 5-1: Spatial profile of peak-to-peak voltage amplitudes of reconstructions investigated at carrier frequencies ranging from 4 to 9 GHz in 1 GHz steps. The inset shows the inverse of the fit b values versus carrier frequency, showing the expected linear relationship.

instrument control and coordination.

5.3 Results

The first experiment measures the spatial profile of a reconstruction, with the goal of characterizing reconstruction size as a function of carrier signal wavelength. A reconstruction is focused on the receiving antenna, in the middle of its movement range. Without changing the time reversed sona being broadcast, the receiving antenna is systematically translated through its entire range of movement. Samples are taken every 0.2 mm across the entire 70 mm range, and the maximum peak-to-peak voltage of the corresponding reconstruction is recorded at each step. We repeated this experiment for carrier frequencies in the range 4-9 GHz and display these results in

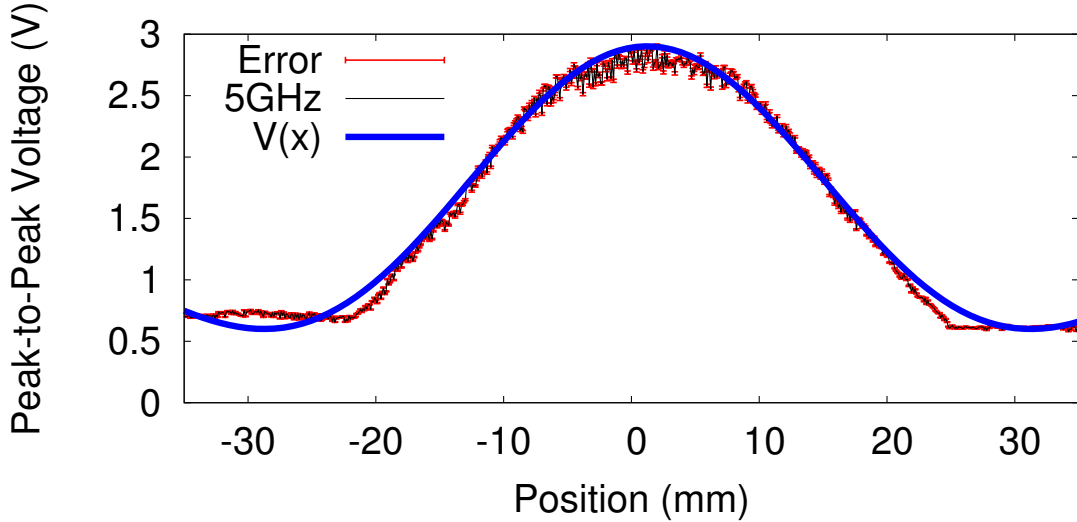


Figure 5-2: Measured peak-to-peak voltage amplitude of reconstructions received in the vicinity of a time-reversed wave collapse location with a 5 GHz carrier frequency, and fit to the $\text{sinc}(x)$ function.

Figure 5-1.

5.4 Discussion

The reconstruction peak-to-peak voltage profile is expected to take the form of a $\text{sinc}(x)$ function about the antenna ???. Thus, the following equation is proposed to predict $V(x)$, the maximum peak-to-peak voltage from a given reconstruction, as a function of x , the distance between the reconstruction focal point and the receiver:

$$V(x) = a \cdot \text{sinc} \left(\frac{x + c}{b} \right) + d \quad (5.1)$$

where a is the maximum peak-to-peak reconstruction amplitude, b is the wavelength of the signal divided by 2, c is the location of the antenna along the x-axis, and d is the noise level offset voltage. Since b is proportional to the wavelength

(and inversely proportional to frequency), as the carrier frequency is increased, $\frac{1}{b}$ also increases, causing the “bubble” of the sinc function in Fig 5-1 to get smaller. This relationship is shown explicitly in the inset of Figure 5-1. Figure 5-2 shows Equation 5.1 fit to the 5 GHz curve from Figure 5-1, including error bars. The fit is good, but has a reduced χ^2 of 234 due in part to the rather large background noise level. The error bars are primarily systematic, introduced by the oscilloscope internal voltage multiplier used in scaling.

Chapter 6

Moving Reconstructions

The TR process assumes that the environment remains fixed between the time-forward and time-reversed steps. It also assumes that the source and target remain fixed between these two steps. We performed time reversal on a moving target to better understand how a translating target affects reconstruction strength.

For this experiment, the receiving antenna moved at a constant speed of $0.5 \frac{mm}{s}$ across the entire 70 mm range provided by the **MikroMove**. To counteract the degradation of reconstruction strength as the antenna moved, we periodically repeated the interrogation step, effectively re-centering the reconstruction on the antenna. Since the test equipment does not allow broadcast of one sona while collecting another, it was not possible to transmit power during the collection time, leading to a finite “dead time”, denoted t_d in Figure ???. During the broadcast period, the time-reversed sona was continually broadcast into the cavity (once every 15 μ seconds) and the peak-to-peak voltage across the receiver was measured once every 2.05 seconds, meaning that the reconstructions are highly undersampled in this plot. After every 15 samples were

collected, we paused to collect a new sona and repeated the process. We refer to this full process of collecting a new sona and then broadcasting it for a given period time as a full “cycle” of length t_c . The results in Fig. 6.1 below were obtained using a carrier frequency of 5 GHz, t_d of 7 seconds, and t_c of 39.8 seconds. Based on the results from Section III-A, the peak-to-peak reconstruction voltage measured by the receiver is expected to decay according to the $\text{sinc}(x)$ function as the receiver moves away from the reconstruction focal point. This $\text{sinc}(x)$ function will be centered on the position where the sona was last collected, making the reconstruction focus continually lag behind the antenna. Consequently, the maximum reconstruction strength is limited by the time needed to collect, time reverse and re-broadcast an updated sona. The following equation is proposed as a model for the peak-to-peak voltage of the reconstruction on a moving target as a function of time, assuming a constant velocity \bar{v} :

$$V(t) = \begin{cases} 0 & : t \pmod{t_c} \leq t_d \\ a \cdot \text{sinc}\left(\frac{\bar{v}t}{b}\right) + d & : t \pmod{t_c} > t_d \end{cases}. \quad (6.1)$$

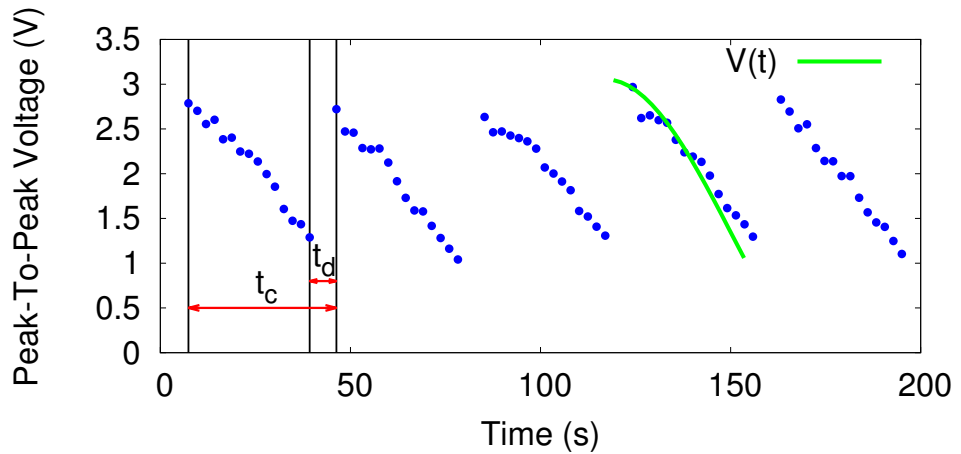


Figure 6-1: Reconstruction voltage amplitude vs. time as the target moves along one wall of the enclosure. A new sona signal is acquired every $t_c = 39.8s$, leading to a dead time of duration $t_d = 7s$. The target is moving at a speed of $0.5 \frac{mm}{s}$ and the carrier frequency is 5 GHz. The green line is Eq. (6.1).

Chapter 7

Methodology for Conducting

Nonlinear Time Reversal

Measurements

The preceding chapters have been concerned with linear time reversal, or LTR, and have focused primarily on investigating properties of reconstructions. Now, we move into our nonlinear/NLTR investigations, which focus on proof of concept of targeting capabilities. As a reminder, NLTR makes use of harmonic reflections from the target to isolate it via frequency domain inspection after the sona is collected, a process similar to how we would envision a TR based WPT system to work.

Conceptually, our general process is this: we broadcast a Gaussian pulse from one port serving as both the transmitter and the receiver. Elsewhere in the Gigabox is a nonlinear element serving as a target. Any reflections from this element

will contain harmonics: frequency components at multiples of the original frequency. These harmonics are embedded along with all the other echos in sona collected back at the transceiving port. However, before time reversing the sona, we transform it into the frequency domain and filter out all the components not within some band of the harmonic frequencies. In this way, we isolate only those wave paths that had contact with the nonlinear target. That filtered sona is time reversed and rebroadcast from the transceiving port, which will cause a slightly distorted version of the original Gaussian pulse to reconstruct at the target. This process is illustrated in Figure 7-1.

We explored several different applications of NLTR with an eye towards adapting the technique for WPT, both experimentally and in simulation. The experimental portions met with limited success due to the difficulty of passively producing harmonics of significant magnitude. However, we believe the the applications of NLTR as a WPT method remains feasible. Discussion of the difficulties that set back our work will be presented in the "Future Works" section in the Conclusion. Successful results, including those of numerical simulations, are explored at length in the following NLTR sections.

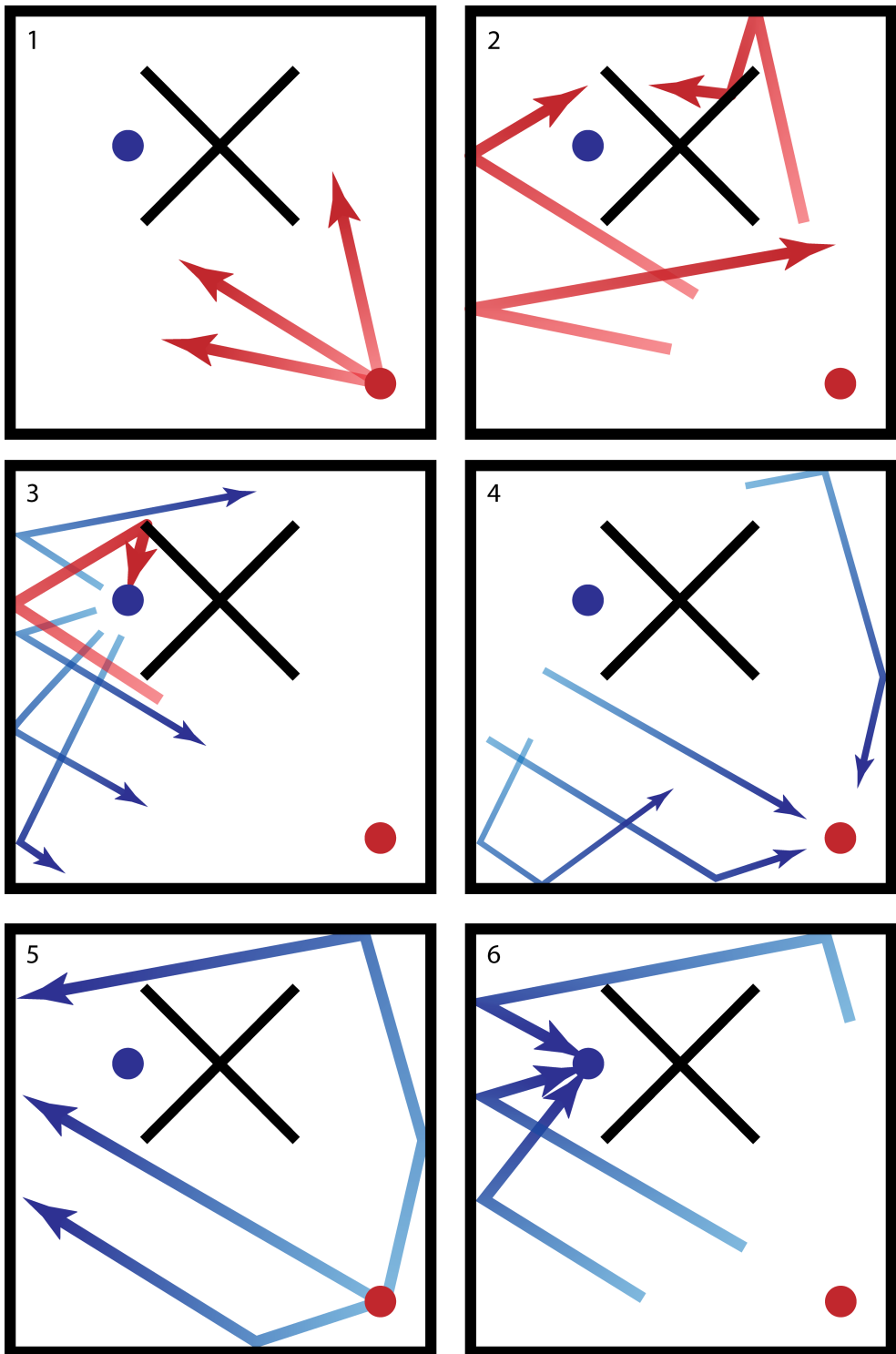


Figure 7-1: Reading order from top left: (1) The TRM broadcasts a signal into the cavity at one frequency, which (2) reverberates within the cavity. Eventually, (3) the signal reaches the nonlinear element somewhere within the chamber. Reflected waves that encounter this element will have a characteristic frequency signature containing harmonics of the original signal. (4) Some of these harmonic reflections will find their way back to the TRM. the TRM filters the sona to extract only those reflections, then time reverses and (5) re-emits them. (6) The time reversed waves collapse back on the nonlinear target.

Chapter 8

Using Nonlinear Time Reversal for Selective Reconstructions

8.1 Purpose

When a WPT system is constructed, it could be advantageous to control which receivers in range are the recipients of electrical power. Linear time reversal is useful for targeting a single device, due to the ability to focus on a single receiver. Tracking several receivers and then independently transmitting them energy poses a significant challenge. Part of this difficulty stems from the fact that the transmitter must have some unique information about the receivers to actually select a desired target. One way to do this is to use receivers which have distinguishing features so the transmitter can select the specific devices. Nonlinear Time Reversal (NLTR) is a version of LTR that creates such distinguishing features in the receivers using nonlinear elements and does not allow unwanted devices to receive more than a negligible amount of energy.

The time-reversal mirror fidelity requires a set of discrete paths between the transmitters and receivers, with neither party knowing the location of the other within the enclosure. The team investigated the case where the receivers differ in their frequency response to an interrogation signal.

8.2 Methodology

To investigate whether a TR technique can demonstrate the ability to distinguish between receiving targets on a basis of their frequency response to an interrogation signal. These experiments were performed within the Gigabox resonant cavity used in the LTR setup above. The AWG, PSG, and DSO setup are used to receive and transmit signals in a manner similar to their use in the LTR setup. The NLTR setup uses three input/output ports; one representing the sender, and two representing different receivers. The NLTR setup is described in Figure 8-1.

The two receivers are designated as either “linear” or “nonlinear” according to their response to a signal at a carrier frequency. The linear receiver responds to the interrogation with a signal at the same carrier frequency as it was queried with. The nonlinear receiver responds with a signal includes the second harmonic of the carrier frequency, in addition to the carrier frequency itself. When an interrogation pulse is transmitted from the sender to both receivers, it is met with a combination of responses at two discrete frequencies; filtering can be used to easily isolate one from the other.

Creating ideal reflector antennas proved to be very difficult given the resources

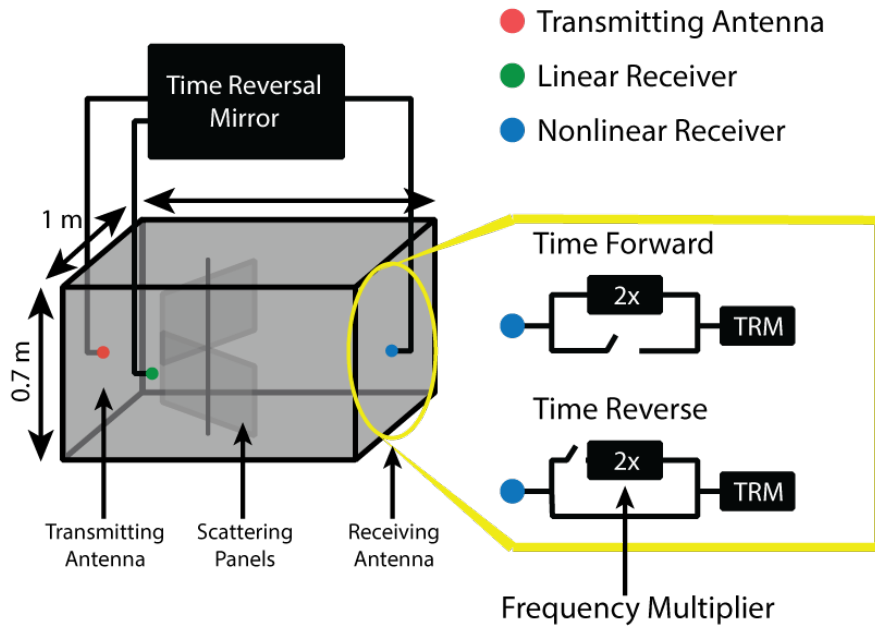


Figure 8-1: Selective Targeting Setup

of the team. Instead of reflectors, an initial signal was broadcast from the receiving antennas. The nonlinear receiver was routed through a frequency multiplier to create the second harmonic needed for NLTR. The sona created by the two receivers was collected at the transmitting antenna. The time reversed sona, broadcast from the transmitting antenna, reconstructs on both of the receivers. One receiver can be targeted separately by filtering the appropriate frequency from the sona, and broadcasting it alone. A reconstruction should appear at the corresponding receiver's port while the other receiver will only detect noise. To ensure that selective reconstruction occurred, the resulting signals at both receivers were monitored and the presence of a reconstruction (or lack thereof) noted.

The experiment was performed with Gaussian interrogation pulses 50 ns in length, at a carrier frequency of 4.2 GHz. The sonas were recorded to lengths of 15 μ s and the signals were broadcast at a power of 3 dBm.

8.3 Results

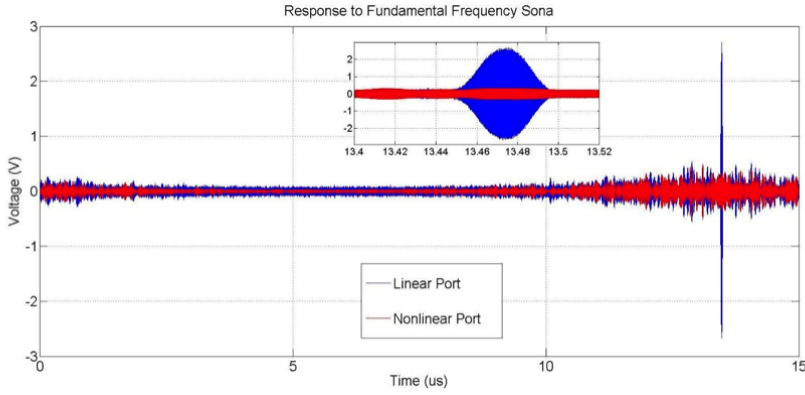


Figure 8-2: Voltage v. Time while Targeting Linear Port

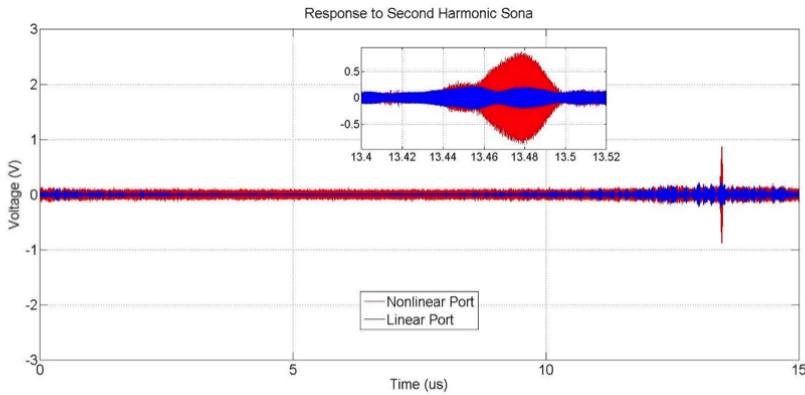


Figure 8-3: Voltage v. Time while Targeting Nonlinear Port

The results of this experiment confirmed the fidelity of the time reversal mirror and its ability to selectively transmit power to a receiver. Monitoring the voltage response of both the linear port and the nonlinear port confirmed the existence of a reconstruction for each case.

When the sona was filtered and broadcast at the linear, carrier frequency, a clear reconstruction emerged at the linear port. At the nonlinear receiver, the lack of a comparable reconstruction is notable. The peak-to-peak reconstruction at the linear

receiver is four times larger than the strongest signal at the nonlinear port, showing that only the intended targets received the bulk of the signal.

When broadcasting the sona filtered around the second harmonic, the opposite effect occurred. The nonlinear receiver received a reconstruction with a peak-to-peak voltage five times greater than the reconstruction at the linear receiver.

8.4 Discussion

This experiment demonstrates the crux of the WPT method proposed by the team. So long as different receivers emit different frequencies of signals, TR can be used to selectively transmit energy to them. In a practical application a transmitter could service a wide number of receivers using this method. Receivers could conceivably alter their nonlinearity to ensure that no interference occurs between them.

There are some further technical challenges that would need to be addressed before this plan can come to fruition however. The primary challenge is that an applied NLTR system would require antennas to reflect the interrogation signals sent to them. The team was unable to create an antenna that had this behavior the the degree desired. Creating nonlinear reflective antennas is an even greater technical challenge. A second challenge is that fine control of nonlinearity is not trivial to do—most changes in nonlinearity generally take the form of integer frequency multiplications. Limited to multiplicative differences will force the bandwidth of an NLTR system to become exponentially large with more receivers.

Chapter 9

Numerical Simulations of the Nonlinear Time Reversal Process

9.1 Purpose

Here, we focus entirely on numerical simulations of NLTR as they apply to WPT. Our focus was threefold: (1) to conduct simultaneous NLTR collapses onto two nonlinear objects, (2) to observe the selective collapse of NLTR onto two distinct nonlinear objects, and (3) to characterize the transmission efficiency of the process. From these three focuses, we demonstrated that the NLTR process may be generalized to an arbitrary number of nonlinear objects in an enclosure and that these reconstructions may be selectively rectified at the nonlinear objects. We provide a scheme to characterize the efficiency of our process but were unable to develop a conclusive theory for tuning the efficiency. Our results provide a baseline for developing an experimental algorithm for targeting objects in an enclosure for WPT applications, either selective

or non-selectively. We will first detail the general scheme used for performing NLTR and follow with the setup, experimental results, and discussion for each of our three focus topics.

The process of developing a new technology required benchmarking each step diligently. Any successful WPT technology must have effective transmission efficiency, implying minimal loss in each step of the system. Given the broad frequency signals used in experimentation, a significant drawback to any TR experiment is the inherent wave reflection at interfaces between equipment, various mediums, or circuitry [28, 16]. While wave reflection losses can be theoretically be measured via S Parameters (explained later) of an experiment, these sources of loss are not practically measurable due to the fact that measuring the losses would create addition interfaces in the system, introducing additional sources of wave reflection [28]. To calculate the true ceiling on effective transfer efficiency, it is necessary to numerically simulate the process, as a simulation can calculate the various losses without interfering with the system itself.

In addition to using simulations to study the sources of loss in our system, it also provided us with a simple nonlinear element—a model diode. As explained in previous chapters, the nonlinear response of in our Gigabox experiments was found to be difficult to excite due to power limitations, noise, or equipment sensitivity. The difficulties that we encountered in our physical experimentation were circumvented by numerical simulating the NLTR process. By being able to monitor the voltage and current response of the diode at all times in the simulation, we were able to troubleshoot problems that occurred in the numerical NLTR process that would have

otherwise have been impossible to determine in experimentation.

9.2 Methodology

9.2.1 Equipment

In order to perform these tests that were not possible in the Gigabox, we used the program Computer Simulation Technology: Microwave Studio (CST for short) to perform electromagnetic wave simulations. CST is an industry standard modeling program that uses the Finite Integration Technique (FIT) to numerically solve Maxwell's equations [31]. This technique is a generalized version of the well-known Finite Difference Time Domain (FDTD) method but can resolve complex geometries and boundary conditions in a simpler manner. We will not discuss these techniques at length, as they are well-understood in the literature [26, 34]. Our team had two computers with a total of two shared CST licenses to perform simulations. The processing power, RAM, and GPU availability are shown below in Table 9.1. CPU A was used for either single simulations or computationally small simulations. A single simulation refers to a simulation where we did not sweep a parameter. CPU B was used for large simulations or parameter sweep simulations, requiring either large amounts of memory or large amounts of time, respectively. In general, we used CPU A to perform simultaneous and selective NLTR while we used CPU B to calculate transfer efficiency and characterize nonlinear response characteristics.

	CPU A	CPU B
Processor	Intel Xeon CPU X5670 @ 2.93 GHz	Intel Xeon CPU E5-2680 @ 2.50 GHz
Number of Processors	2	2
RAM	44 GB	128 GB
GPU Available	No	Yes

Table 9.1: Technical specifications of the computers used for conducting all simulations and modeling.

9.2.2 Time-Reversal and Nonlinear Sona Extraction

To start any simulation, we first generated a Gaussian pulse signal in MatLab. For this interrogation signal, we chose the amplitude, center frequency, and bandwidth frequency for our experiment. An example input signal is shown inset in Figure 9-1. The simulation was run using this pulse signal, noting one of the ports as an injection port (e.g. Port A) and one as the recording port (e.g. Port B).

In general, we had two methods to extract the nonlinear sona from our recorded signal: (1) applying a Fourier transform and band-pass filtering the raw signal and (2) pulse inversion. As previously discussed, many of the Gigabox experiments were performed by recording a sona, applying a Fast Fourier Transform (FFT), and finally using a band-pass filter on the recorded signals to extract the harmonic signal at the correct frequency. In our numerical simulations; however, the sonas were only recorded for 30–35 ns and the discretized nature of the data on this time scale led to distortion of the sona signals. The team also explored using another method of sona extraction that has been well documented in the literature [27, 18]. Hong et al. have

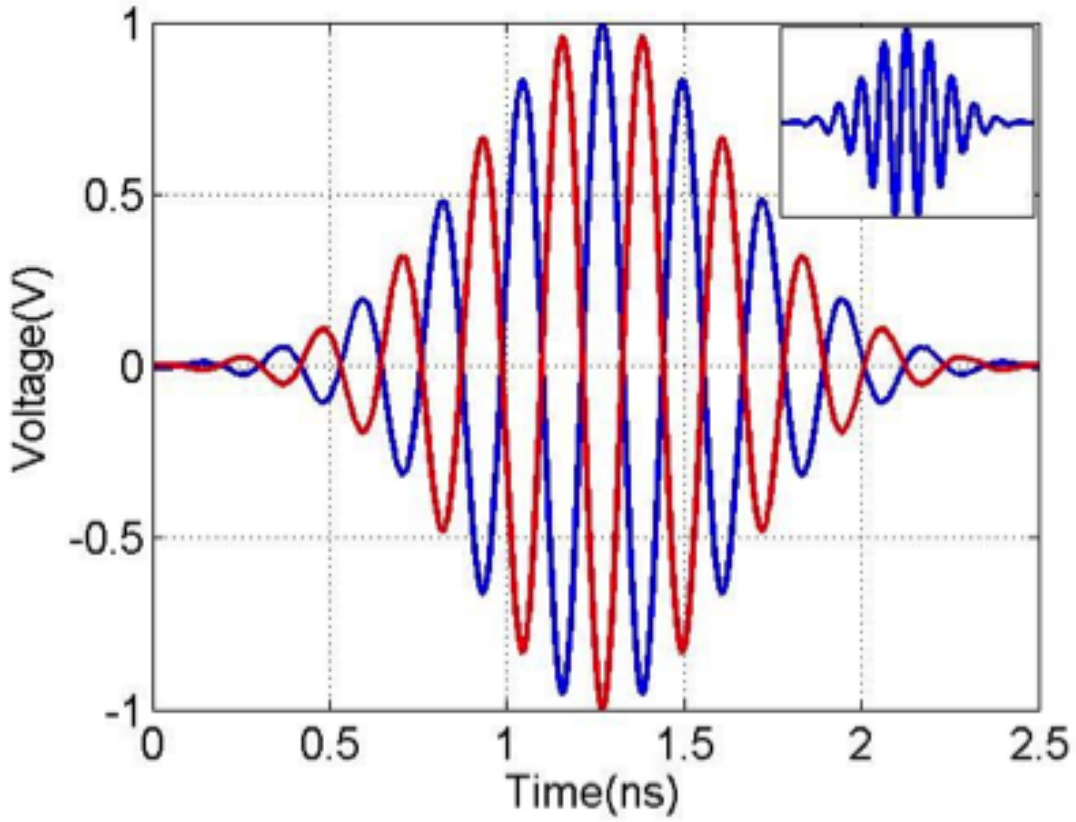


Figure 9-1: This shows our input waveform with a 4.4GHz center frequency and 1.0GHz bandwidth. The blue signal is the non-inverted input and the red signal is the inverted input. A singular, non-inverted waveform is shown in the inset.

used this method for numerous time-reversal experiments, citing its computational simplicity as a benefit for using it in physical experiments [18]. The process involves summing two signals, rather than applying a transformation to an entire sona signal, saving time. While this process proved to be very difficult for our Gigabox experiments, it was quite efficient at producing the nonlinear sona in CST. Due to the simplicity of pulse inversion, we used this method for extracting all nonlinear sonas. In this method, we ran the same simulation once with our original input signal and then we ran it a second time with an inverted version of our original signal. Inversion simply means that the entire original signal was multiplied by -1 . Assuming

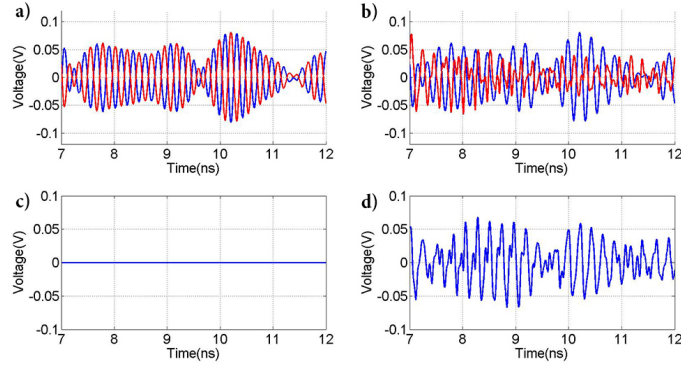


Figure 9-2: (a) shows a portion of the non-inverted (blue) and inverted (red) recorded response signal. (b) shows the same two response signals when a diode is present in the simulation. (c) the sum of the two signals in (a), resulting in signal annihilation. (d) the sum of the two signals in (b), which produce a non-zero signal.

a linear system, the sum of the original and inverted signals sums to 0; however, a nonlinear system sum is non-zero. Because the diode is the only nonlinear portion of the system, summing the original and inverted signals yields only the signal from the diode, which is the desired nonlinear sona. Figure 9-2(a) and (b) illustrate two sona signals, where the blue signal is the non-inverted sona and the red signal is the inverted sona. Figure 9-2(b) contains a nonlinear element while 9-2(a) does not. The corresponding (c) and (d) show the result of summing the two signals. It is clear that total annihilation of the sona signal occurs when no nonlinear element is present, as in 9-2(c), while a clear signal is present in 9-2(d).

This method to extract the nonlinear sona was chosen over taking the FFT and filtering the recorded signal as sample rate for the simulation data was not high enough to ensure the results would not be distorted. This discretization of data caused the resulting time-reversed sonas to produce incorrect results using the FFT and filter method, while the time-reversed sonas produced correct results with the

pulse inversion method.

9.2.3 Defining and Controlling the Nonlinear Element

In the simulations themselves, we used a model diode as our nonlinear object, as it has a nonlinear I-V curve. The diode location for each simulation was chosen semi-arbitrarily with the only restriction to not be within 1–2 wavelengths of either port, as this may have created near-field effects that influenced the results. In CST, the diode component is modeled as the following circuit (Figure 9-3) and mathematical relationship (Equation 9.1 and 9.2). From these, the user may change the parasitic capacitance (C), the series resistance (R), the reverse conductance (G_s), and the functional temperature (T).

For $V_d > 0$:

$$I_d = I_0 \left(e^{\frac{eV_d}{kT} - 1} \right) = I_0 \left(e^{\frac{V_d}{V_k} a - 1} \right) \quad (9.1)$$

For $V_d < 0$:

$$I_d = G_s V_d \quad (9.2)$$

To obtain idealized results, we set C and G_s to 0, as these values reduced the magnitude of the nonlinear response. We used the default $R = 50\Omega$, as very large R reduced the overall signal greatly and a very small R did not produce any harmonics. This left only T to tune the I-V curve of the diode. In real life, different diodes have different I-V curves based on material. In order to simulate these differences

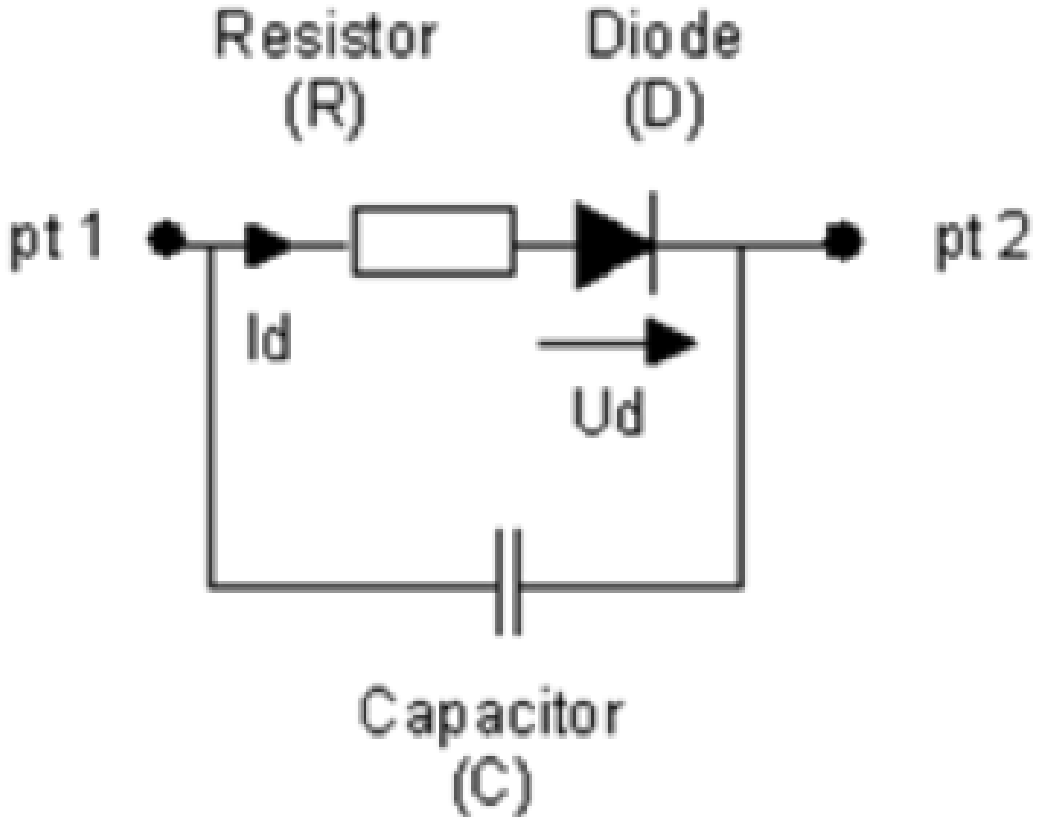


Figure 9-3: CST circuit model of a diode.

mathematically, we changed the temperature of the diode in the simulation, as shown in Figure 9-4.

In reality, this changed the knee voltage (V_k) for the diode. We chose V_k to be the applied voltage needed to achieve a current of $0.2I_0$. The parameter a is used to define this $0.2I_0$ cutoff. As discussed later in this chapter, we will show how the nonlinear response of a diode is dependent on both the input pulse amplitude and the knee voltage. This nonlinear response was maximized to allow for selective targeting between two diodes simultaneously.

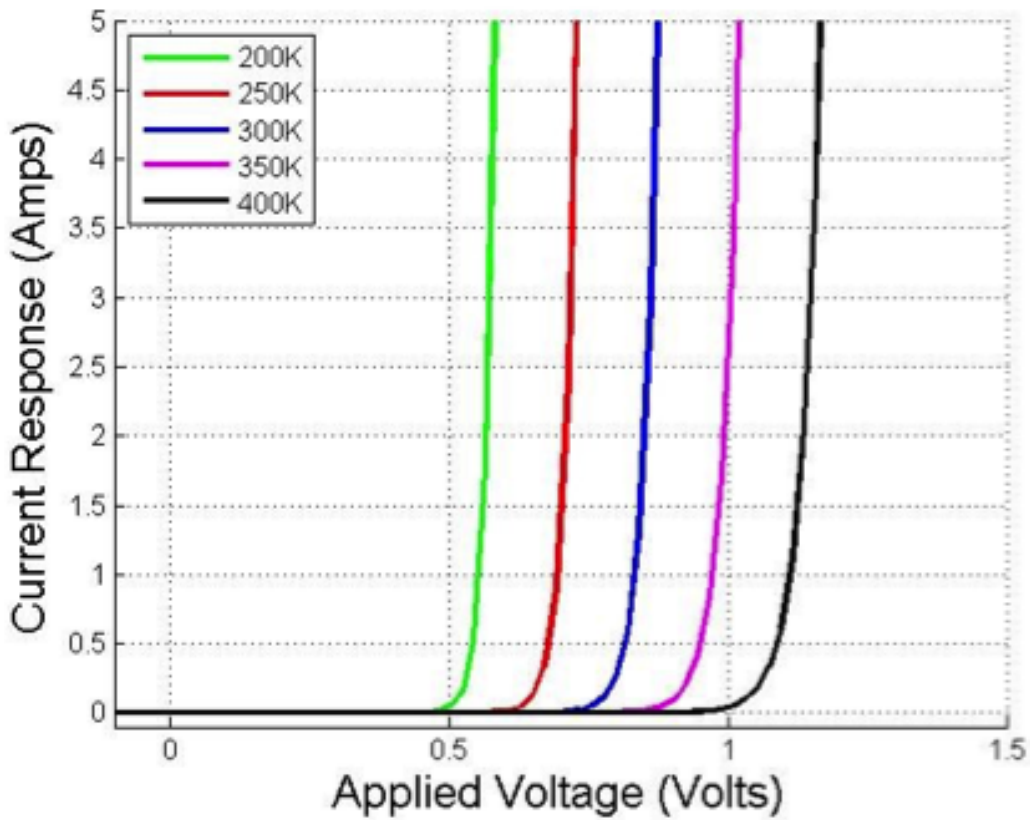


Figure 9-4: Different I-V curves that can be modeled in CST. It should be noted that the “Temperature” of the diode only changes its mathematical definition of the I-V curve

9.3 Results

9.3.1 Simultaneous Nonlinear Time Reversal

The first focus of our numerical simulations was to illustrate the collapse of a nonlinear time-reversed sona on multiple targets simultaneously. To be an effective WPT system, our technology would need to be able to charge more than one device at a time. Based on literature illustrating NLTR collapsing on a single nonlinear object, we hypothesized that a nonlinear sona would collapse on an arbitrary number of nonlinear objects if the nonlinear objects were present in the time-forward step of

NLTR [15, 14]. We assumed that the reconstruction on each nonlinear object would sum linearly and independently such that no reconstruction would interfere with another, as shown in Equation 9.3, where R_i is the reconstruction on a single nonlinear object and x_i is a weighting of the amount of power that the single nonlinear object contributes to the overall power of all reconstructions. Based on this, we expected the reconstruction waveforms of the independent single-diode simulations to match a single, multi-diode simulation.

$$R_{tot} = \sum_i R_i x_i \quad (9.3)$$

This feature was realized by creating a geometry with two diodes present along with two ports to record and emit signals, shown below. We created a quasi-two-dimensional (2D) irregular cavity in CST. This cavity was a 15cm x 15cm x 0.76cm square box modified with various circular and elliptical segments removed from the walls as shown in Figure 9-5. The 0.76cm height was chosen to maintain a 2D simulation. Equation refeq:numerical-cutoff-freq was used to calculate the cutoff frequency for the fundamental mode of a parallel plate cavity, below which only 1 frequency will propagate, reducing the time needed to simulate [16].

$$f_c = \frac{c}{2h} \quad (9.4)$$

Using a cavity of height 0.76 cm resulted in a cutoff frequency of 20 GHz, well above our typical test frequencies of 4-5 GHz fundamental and 8-10 GHz harmonic.

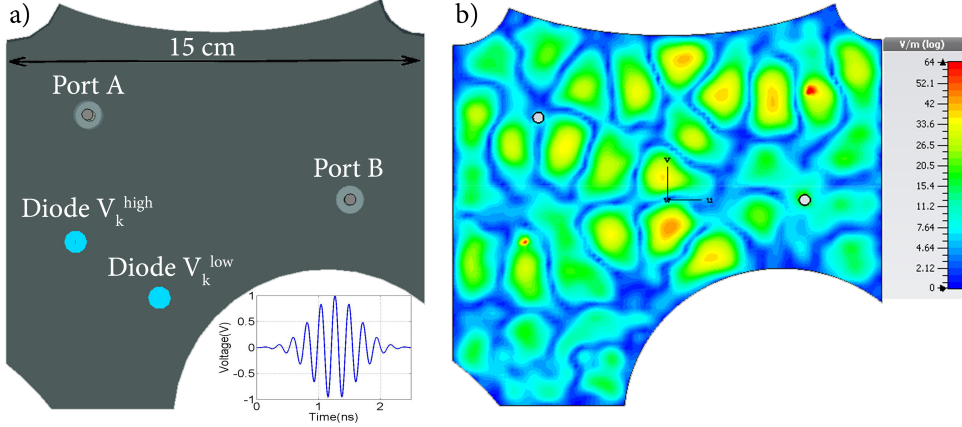


Figure 9-5: The Cut Box simulation geometry used in CST. (a) shows the location of the 2 ports (A and B), 2 diodes (V_k^{high}, V_k^{low}), length scale, and the lower inset shows the initial interrogation pulse. (b) shows the electric field at a point in the simulation, illustrating the limited excited mode density.

We chose this cutoff frequency in the event we needed to use a higher fundamental frequency to create better spatial resolution of our reconstruction. The area dimensions for the Cut Box Model were chosen to minimize computational time while still maintaining a reasonable mode density, as shown in Figure 9-5(a). This mode density is required to allow the ray chaotic environment to have high sensitivity to initial and boundary conditions; a low mode density will prevent NLTR from having high spatial resolution.

We used two Teflon-coated dipole antennas to emit and record signals [17]. Two diodes are placed inside the cavity, shown by the blue circles in Fig. 5. A 4.4 GHz center frequency pulse with a 1.0 GHz bandwidth was chosen to minimize the reflected power and applied to antenna A. The interrogating pulse is shown as an inset in Figure 9-5(a).

The specific frequency and bandwidth was chosen for this geometry to minimize initial wave reflection (S_{11}) into the enclosure. Figure 9-6 shows that using a 1

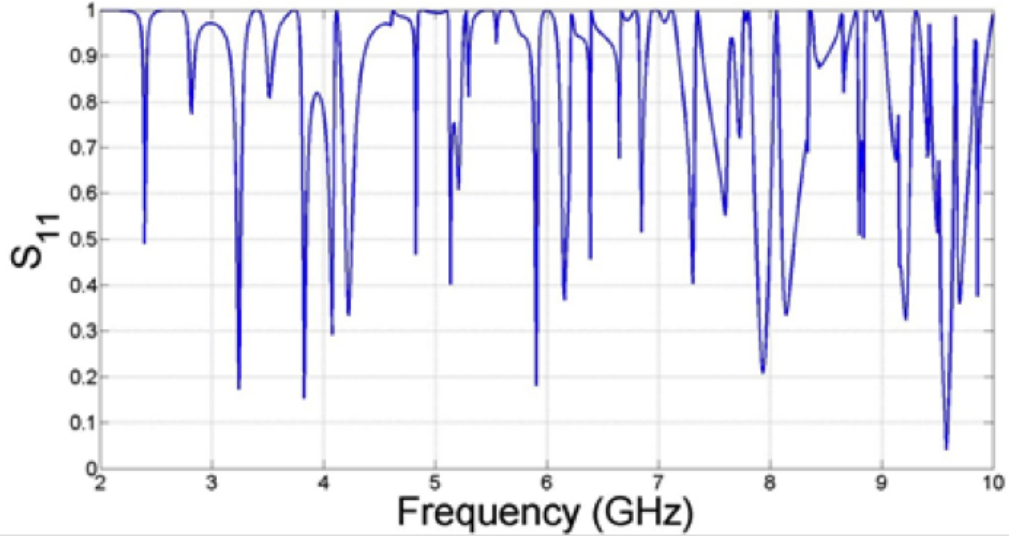


Figure 9-6: The S_{11} spectrum for the Cut Box Model. We wanted to minimize S_{11} for our simulation while maintaining a large bandwidth. This led to choosing a 4GHz center frequency with a 1GHz bandwidth.

GHz bandwidth, an optimal center frequency is 4.4 GHz. The dips in the S_{11} value represent optimal frequencies to use, as a low S_{11} indicates a large portion of the signal entered the cavity. The large number of peaks is indicative of the mode density of the geometry, where low frequencies are sparse given the relatively small scale of the cavity.

Using this input pulse and the pulse inversion method of sona extraction, we were able to perform NLTR in the Cut Box Model. By measuring the observed voltage and corresponding current during the time-reversed step, we measured the quasi-power over time in each diode. As shown in Figure 9-7, the reconstruction waveform on each diode matches the expected results for a 1-diode experiment [30, 6].

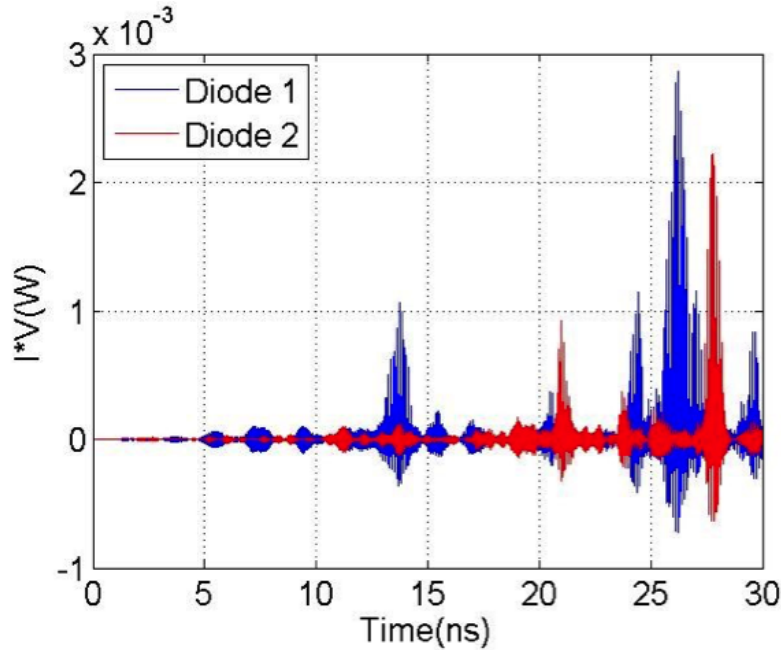


Figure 9-7: The time-reversed reconstruction on two diodes simultaneously performed inside the Cut Box geometry.

9.3.2 Discussion of Simultaneous Nonlinear Reconstructions

This result alone signifies the generality of NLTR whereby any nonlinear object in the cavity will observe a reconstruction in the time-reversed step. In regards to a larger WPT system, one can imagine that this is particularly useful inside of a home or public area, where any device may be powered as long as it is within range of the transmitter/receiver base station. Because the process used only creates a reconstruction at the nonlinear element, it is as simple as repeating the NLTR process rapidly, creating a quasi-pulse width modulation (PWM) signal that can charge a battery. PWM is a method for controlling how active a device is by rapidly switching the device on and off. For example, a fan has different speeds because it operates 25%, 50%, 75%, or 100% of the time. Similarly, if we can reconstruct on a battery circuit every 10% or 20% of the time, we can effectively charge the battery. As soon as

the nonlinear object leaves the enclosure, it will no longer receive power. By having a base station that can actively modulate output sona power, it would be very simple to change the amount of power transferred to each device. This dynamic power control is outside the scope of our project but represents a much later extension to this WPT system.

9.3.3 Simulation of Selective Collapse of NLTR

The logical next step is to determine how such a system would be able to determine which device should be powered. As previously shown, if nothing is done to alter the sona signals, then the sona from each nonlinear object will sum linearly and produce a reconstruction at all nonlinear objects in the time-reversed step. Given that each reconstruction sums independent of one another, we hypothesize that we should be able to eliminate the contribution of one nonlinear reconstruction to the overall set of reconstructions without altering the fidelity of any other individual reconstruction on other nonlinear elements. For example, in an enclosure with 3 diodes, if we could suppress the response of diode 2 in the time-forward step, then we would expect to only observe a reconstruction on diodes 1 and 3, creating a selective targeting method. Using Eq. 3, this would imply a weight of $x_2 = 0$, as shown in Equation 9.5.

$$R_{tot} = \sum_i R_i x_i = R_1 x_1 + R_2 * 0 + R_3 x_3 = R_1 x_1 + R_3 x_3 \quad (9.5)$$

In a commercial setting, this would be an extremely useful aspect to our WPT system, as companies could require payment to use the system and would otherwise

suppress the reconstruction on the user’s device. The fact that the nonlinear object is passive in the environment implies that this selective targeting could even be used to “resurrect” a dead phone, a feature not seen on any current WPT technology on the market.

We have developed a method of performing such a targeting scheme based on the previously mentioned diode model. In the simplest case, we show that selective targeting for 2 diodes with two separate voltage knees was obtained (noted V_k^{high} and V_k^{low}).

Recall the current response in the diode from Equation 9.1. One useful aspect to the diode definition function is that if $V < V_k$, then the diode has very little current response, which in turn implies a low nonlinear response. We utilize this characteristic while performing selective targeting on a low V_k diode. Similarly, we observe that at small V_k values, the nonlinear response is small. These two observations led to the hypothesis that nonlinear response may be maximized given an initial pulse by selecting a proper V_k value. As shown below, Figure 9-8 was obtained by sweeping over many V_k values for different initial pulse amplitudes given the same geometry and process conditions as previously stated. Given this distribution, we may target a high V_k diode, as the nonlinear response will be stronger in the high V_k diode than the low V_k diode.

To perform this selective targeting, we once again used the Cut Box Model. In the simplest case, we consider selective targeting of a low $V_k = 0.79V$ (V_K^{low}) diode at the exclusion of a high $V_k = 6.60V$ (V_k^{high}) diode. Given the large value of V_k^{high} , we expect to see no response in that diode while maintaining a reasonable nonlinear

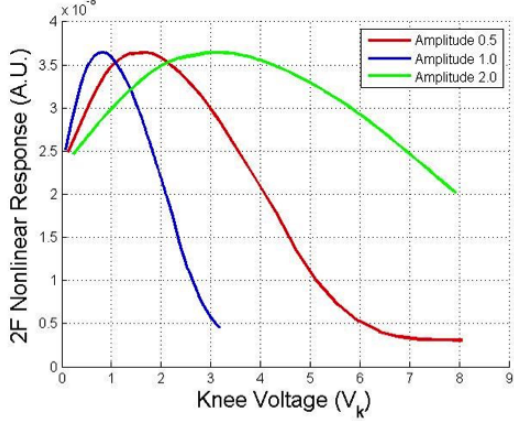


Figure 9-8: The nonlinear response of the diode had a clear maximum at a specific knee voltage. By using a pulse amplitude that corresponded with the specific diode knee voltage, we could selectively target diodes in CST.

response in the V_k^{low} diode. We used a pulse with amplitude $V = 1.0V$ during the time forward step, emitted at Port A in Figure 9-5(a). Using pulse-inversion, we extracted the nonlinear sona from the recorded signal at Port B, time-reversed the signal, and re-emitted it from Port B. Figure 9-9 shows the time-reversed reconstructions on both diodes. This results in a reconstruction almost exclusively on the V_k^{low} diode during the time-reversed step. The presence of three reconstructions when only one initial pulse was not alarming, as short-orbit paths between Port A, the diodes, and Port B that carry enough power to excite the diode harmonics are known to exist [?]. To calculate the quality of the selective reconstruction, we determined the aspect ratio by comparing the max of IV on both diodes. For this scenario, we calculate a power delivery aspect ratio of 6.35:1 for the V_k^{low} diode relative to the diode with V_k^{high} .

The more difficult scenario was to selectively target a high V_k diode at the exclusion of a low V_k diode. We utilized the peak in nonlinear response as a function of knee voltage from Figure 9-8. By choosing the correct pulse amplitude corresponding to a

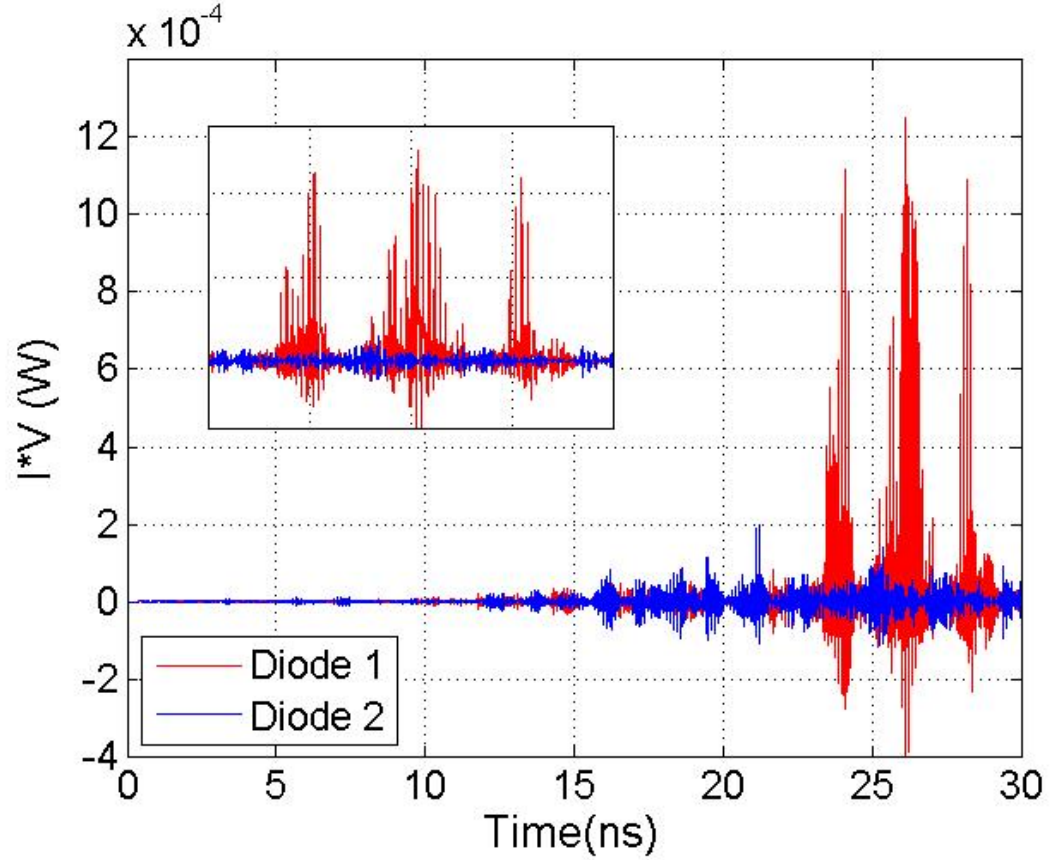


Figure 9-9: Time-reversed reconstructions on the two diodes while targeting V_k^{low} . Very little signal is seen on the V_k^{high} diode. The insert shows the details of the reconstructions between 22 and 30 ns.

peak value that was matched to the high V_k value, we expected to see the strongest nonlinear response, resulting in the largest magnitude reconstruction. In this scenario, the low V_k diode still observed a reconstruction; however, it was smaller in amplitude than the high V_k diode reconstruction. Given that a real system would involve a full rectification circuit in addition to the diode, the smaller amplitude reconstruction may not be able to turn on the rectifier while the high amplitude reconstruction at the high V_k diode would turn on. For our simulations, we were able to model this by measuring the observed power ($I * V$) on the diode and modify the sona amplitude in order to ensure the V_k^{high} diode had rectification while the V_k^{low} diode did not.

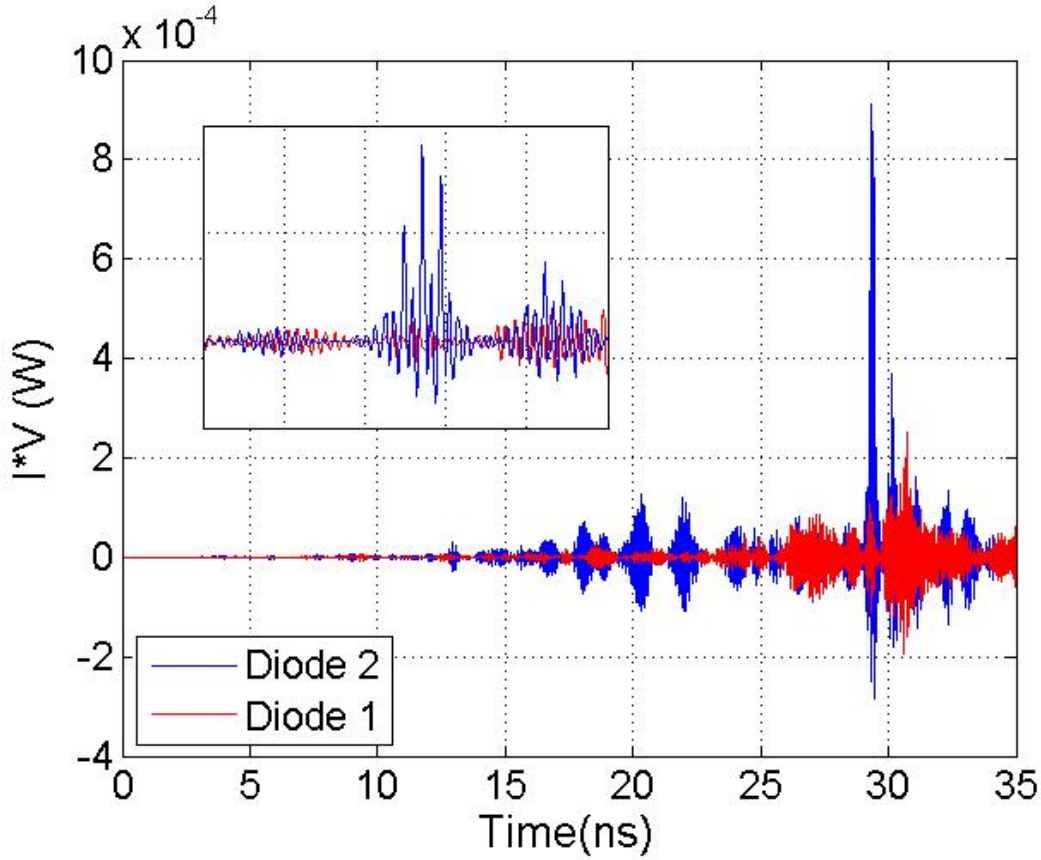


Figure 9-10: Time-reversed reconstructions on the two diodes while targeting V_k^{high} . Sona amplitude modulation resulted in a clear contrast between the two signals.

For this second scenario, with $V_k^{high} = 2.22V$, we once again used an amplitude 1.0V pulse during the time-forward step so that we may compare the results from both scenarios equally. As shown in Figure 9-10, pulse amplitude of 1.0 has a maximum nonlinear response at 2.22V. We chose this V_k value, as it gave the clearest reconstruction. Once again, we used pulse-inversion to extract the nonlinear sona. In general, this results in a larger magnitude reconstruction on V_k^{high} . This contrast between the V_k^{low} and V_k^{high} reconstructions was amplified by modulating the time-reversed sona amplitude, such that the reconstruction voltage seen at the target diode was barely larger than V_k for V_k^{high} and just barely smaller than V_k for V_k^{low} . This

resulted in selectively reconstructing on V_k^{high} only during the time-reversed step with an aspect ratio of 3.61:1 for the V_k^{high} diode relative to V_k^{low} , as shown in Figure 9-10.

9.3.4 Discussion of Selective Nonlinear Time Reversal

We have demonstrated a basic method for creating selective rectification using NLTR to target different nonlinear objects. This represents a stepping stone from the previously shown method of generalizing NLTR. By altering the input pulse amplitude, we were able to achieve the hypothesized nonlinear response suppression of specific nonlinear elements. This shows that the nonlinear reconstruction created on each nonlinear element is independent of one another and may be modified without impacting the other elements of the overall reconstructions. We have shown that this WPT technology would be capable of ubiquitous charging on any nonlinear device as well as selective targeting of specific devices. One may think of this as having an NLTR charger in one's home compared to having an NLTR in a business. In a domestic setting, there is very little need to restrict access to power. There are many outlets in one's home and there is no need to tell someone they are not permitted to use it. In a business however, a power outlet is not available to customers unless they pay for it. In this case, it is very useful to be able to selectively choose who may receive power. Although we have not shown a full-fledged system to do so, we have presented a foundational process that may be improved upon in order to create a successful NLTR-based WPT system.

9.3.5 Simulation of Transmission Efficiency of NLTR Process

We have so far shown that NLTR may be used in a WPT system to either power all nonlinear objects or selectively target the nonlinear objects within a relevant range. One significant question though that arises is to what efficiency are these objects powered. Surely a system that can only transfer 2% of applied power will not be a successful WPT technology, as the consumer is paying for the luxury to not carry around a cable. If the user has to pay 50x more for the power they are very unlikely to use our system. As previously discussed, energy losses are often difficult to calculate in real experiments due to wave reflection and other systematic sources of error. However, by simulating the NLTR process, we are able to observe approximate transfer efficiency. In CST, we are able to track input power and power loss via wave reflection, absorption in both lumped elements and environment materials, and radiation loss at other ports. One drawback to using the built-in CST power tracking is that everything is recorded in the frequency domain rather than time domain. For example, a typical power spectrum from a time-reversed step of a 2-diode NLTR simulation is shown in Figure 9-11. As we are interested in overall power input compared to overall power output, we used this data along with Equation 9.6 to compute the efficiency of transfer in our simulations.

$$e = \frac{\sum_i P_{i(diode)}(f)}{\sum_i P_{i(input)}(f)} \cdot 100 \quad (9.6)$$

The above data was taken from a simulation in the Cut Box model for the previously discussed two-diode simultaneous reconstruction. For this simulation, we found

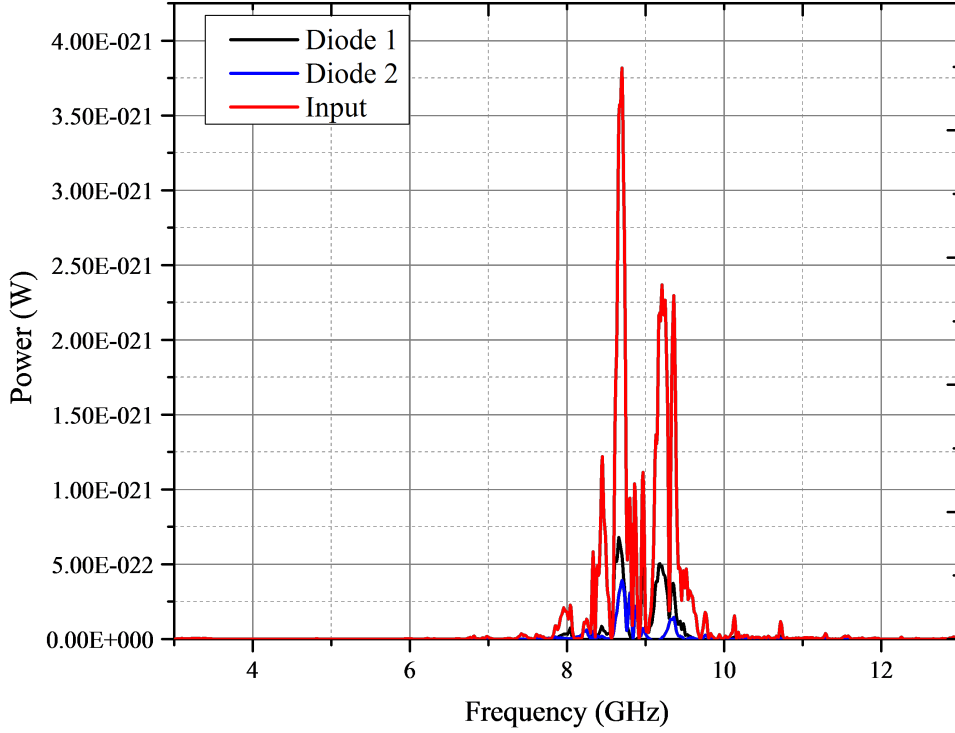


Figure 9-11: A typical power spectrum obtained in the time-reversed step (reconstruction). The power that enters the diodes only represents a portion of the overall power input in the simulation.

that 18.6% and 7.3% of power were transferred from the nonlinear sona to diodes 1 and 2, respectively. This provides a promising outlook.

Our next question was whether or not these transfer efficiencies were a function of distance between transmitter port, diode, and receiver port. We found that using similar diode positions as previously stated resulted in transmission values around the 7–18% shown above. We decided to introduce a new model with a much larger length scale, called the Room Model shown in Figure 9-12.

We chose to use a 45cm x 45cm x 0.76 cm initial box to simulate a large geometry while still maintaining a quasi-2D cavity. The 45 cm length scale was used, as any

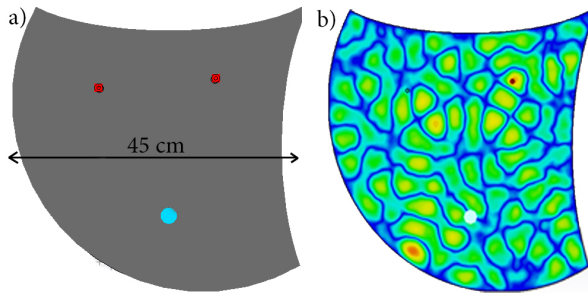


Figure 9-12: Illustrates the geometry of the simulation.

larger simulation ran out of memory prior to completion. Due to the length of simulation and decreased nonlinear signal strength, this model was unable to be used for further efficiency calculations. From Figure 9-12, the distances in the simulation are much larger than the Cut Box and may be used in the future to determine whether transmission efficiency of NLTR is dependent on distance between transmitter, nonlinear object, and receiver ports.

9.4 Conclusion

Using CST, we have successfully demonstrated our 3 goals: (1) simultaneous reconstructions on multiple nonlinear objects (2) selective reconstructions between multiple nonlinear objects and (3) calculation of a baseline transmission efficiency of NLTR. For simultaneous and selective targeting, we provide a basic framework to perform these processes using numerical simulations; however, these processes are still yet to be performed in real-world experimentation. We believe that this illustrates a foundational work for future experiments to demonstrate the feasibility of these features in a new WPT technology. Additional research must be done in order to character-

ize the ceiling on transmission efficiency if NLTR is to be applied to a future WPT technology.

Chapter 10

Ferromagnetic Nanorods as a Nonlinear Beacon

10.1 Purpose

As noted in Chapter 8, the team faced significant difficulties creating a nonlinear signal for use in NLTR. The team investigated the use of ferromagnetic nanorods to generate a nonlinear signal.

10.2 Methodology

An additional experiment was conducted by the team to determine whether ferromagnetic nanorods could generate a useable nonlinear signal for nonlinear time reversal. For the first experiment, the ferromagnetic nanorods were attached with tape to a monopole antenna and put into a small box lined with tin foil that acts as a reflective

chamber. This was attached via a circulator in sequence with a signal generator and a spectrum analyzer (as shown in Figure 10-2). The signal generator output a CW, which swept from 1–10 GHz every .5 GHz.

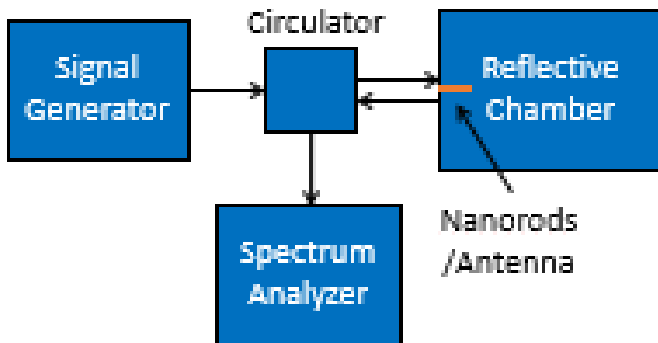


Figure 10-1: Diagram showing connections between the antenna, signal generator, and spectrum analyzer used in the first experimental setup.

The next step in this research was to move to Gigabox testing. The setup for this experiment followed that of the first step of linear time reversal, with modifications to the responding antenna depending on the iteration of the variable being tested.

In the first round of testing, a simple pole antenna was used, with the ferromagnetic nanorods being taped to the transmitting antenna. The DSO then collected the signal from the transmitting antenna at a port several centimeters away.

After initial tests with the control variable being the presence of the ferromagnetic nanorods, the next test compared the base behavior of the antenna to the response of the ferromagnetic nanorods in the presence of a magnetic field. In order to accomplish

this, a magnet was affixed to the outside of the Gigabox as close to the transmitting port as possible. In each of these first two tests, the frequency was swept every .1 GHz from 3.5 GHz to 6.5 GHz.



Figure 10-2: The ferromagnetic nanorods are affixed inside the copper solenoid, which is placed beside the antenna in order to test a different alignment of the magnetic field.

The third and final test relied on the same magnetic stimulation as the second iteration of the Gigabox test, with a different antenna, this one fashioned into a solenoid, to test a different alignment of the magnetic field. This final round of testing had the highest frequency resolution, which swept from 3.05 GHz to 6 GHz at every .05 GHz. For additional certainty, the measurements from five runs were averaged for a final result.

In each of the above tests, the carrier frequency was the independent variable swept across. This is represented as 1F. The dependent variable was the recorded

voltage at the nonlinear frequency, $2F$, double the carrier frequency. This voltage was separated using an FFT function in Matlab.

10.3 Results

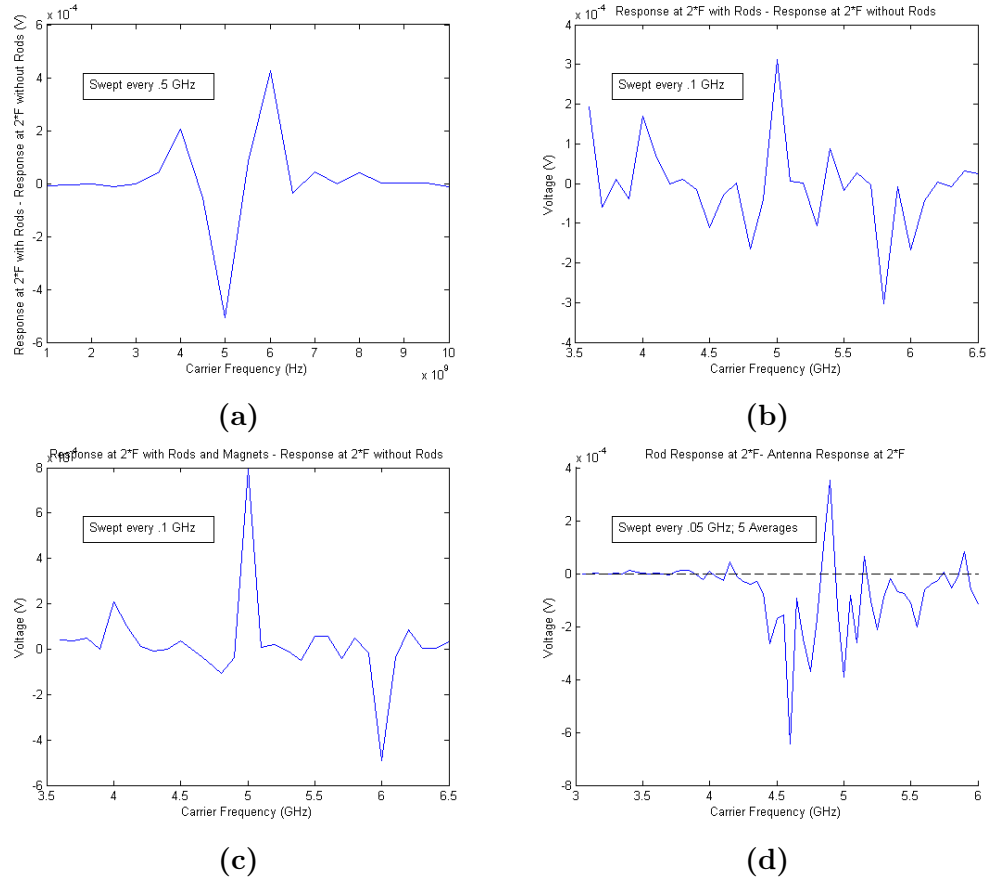


Figure 10-3: Experimental results

Figure 10-3a shows positive spikes in nanorod response compared to the base at 4 GHz and 6 GHz. Contrast this to Figures 8 and 9 below; they show a sharp peak in nonlinear response with the ferromagnetic nanorods at 5 GHz, where the sharp dip in performance occurred in the first test.

Figure 10-3d shows the final results with the loop antenna and magnetic stimula-

tion, with behavior averaged across five tests. This is also the finest resolution, taken in the areas of interest from the results of the previous tests.

10.4 Discussion

The results show a general attenuation response in the gigahertz range of transmission for the ferrite ferromagnetic nanorods. The first test involving the small foil-lined box showed an extremely attenuated response at all frequencies. The level of attenuation seems to indicate that the ferromagnetic nanorods have no significant nonlinear response. Higher frequencies might provide a more significant response, though this would require different equipment than what is currently available.

Chapter 11

Development of a Super Rectenna

11.1 Goals of Rectenna

One of the main components of any WPT system is its rectifier, as it performs the crucial step of capturing the broadcasted energy and transforming it into a usable form. To accomplish this, a rectenna, a dual-purpose device that combines an antenna and a rectifier, is necessary. The antenna picks up the unusable, oscillating AC signal received from the transmitter, the rectifier converts the signal to relatively stable DC power, and this usable power is passed to an arbitrary load.

In addition to standard rectification, the rectenna must serve as a passive nonlinear element. In NLTR, a nonlinear element is required to produce harmonics from the initial interrogation pulse broadcast by the transmitter. However, this goal is secondary to the main purpose of rectification.

The rectenna was designed to fit the following parameters. First, the rectenna must operate efficiently at the high frequency (1–10 GHz) required for efficient NLTR.

Additionally, losses due to reflection and parasitic effects within the antenna should be minimized. Finally, to fulfill the role of a nonlinear element, the rectenna should generate distinguishable harmonics strong enough for the purposes of NLTR.

In short, to rectify and generate harmonics for NLTR, the rectenna must be capable of not only efficient rectification at high frequencies, but also production of strong harmonics for NLTR.

11.2 Diode Selection and Testing

The diode is the most important single component to consider for the rectenna, as it is the main rectifying component. Careful consideration of its characteristics is vital. The switching frequency, forward voltage drop, and impedance of the diode are of particular importance to the desired goal of efficient rectification.

For the rectenna in our design to perform efficiently, the diode must satisfy several requirements:

The diode must maintain functionality as a diode at a transmission frequency of 1–10 GHz, and must rectify at a frequency of at least 10 GHz. This requirement severely limits the possible choices for the rectenna diode. The frequency of a diode is inversely related to its reverse-recovery time (TRR), the fastest time the diode can switch from forward to reverse bias [4]. In traditional P-N junction diodes, minimum TRR is on the order of tens to thousands of nanoseconds, even for fast diodes [12]. In a high frequency circuit, a P-N diode would be no different than a short circuit, and no rectification would occur.

The diode must have the lowest forward voltage drop possible. The voltage drop represents the reverse bias that remains when the diode works in the forward direction, and can be a significant contributor to power loss. The team's experimental WPT capabilities are limited to fairly low voltage microwave signals (.5 V to 1 V signal amplitude), which makes forward voltage drop especially important.

Finally, impedances should be minimized to reduce loss. All diodes have intrinsic impedances such as parasitic capacitance and resistance. Impedances contribute to losses during rectification and destabilize circuit behavior, resulting in unpredictable behavior.

Considering these factors, a Schottky barrier diode were chosen for the rectenna. Unlike P-N junction diodes, Schottky diodes have extremely low TRR and low forward voltage [12]. Schottky diodes do have a lower maximum reverse voltage rating, higher reverse leakage current, and higher cost than P-N diodes. However, these are relatively minor issues in our application. A Schottky MA4E1317 diode was used as the rectifying diode. The diode parameters from the are shown in Table 11.1.

The MA4E1317 has low total capacitance (.045 pF) and series resistance (4Ω), minimizing parasitic losses. The datasheet also cites an operating frequency of up to 80 GHz for this diode, more than sufficient for our purposes. The forward voltage cited to be around .7 V, a typical value for most diodes [21]. A lower forward voltage would be desirable, and in considering future improvements to the system, this is definitely a point to consider.

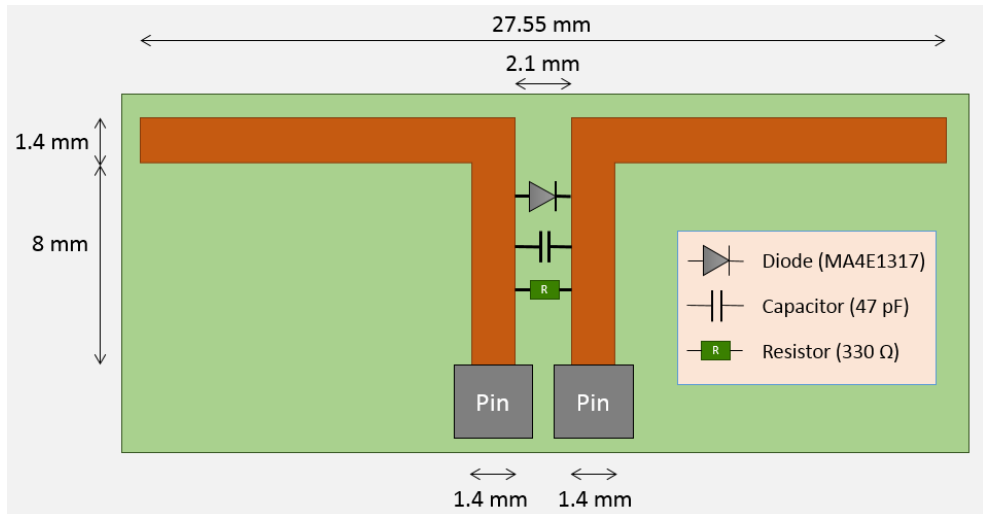
Test Conditions	Symbol	Units	Min.	Typ.	Max.
Junction Capacitance at 0 V at 1 MHz	Cj	pF	-	.020	-
Total Capacitance at 0 V at 1 MHz	Ct	pF	.030	.045	.060
Junction Capacitance Difference	DCj	pF	-	-	-
Series Resistance at $+10\text{ mA}^2$	Rs	Ω	-	4	7
Forward Voltage at $+1\text{ mA}$	V_{f1}	V	.60	.70	.80
Forward Voltage Difference at $+1\text{ mA}$	DVf	V	-	-	-
Reverse Breakdown Voltage at $-10\mu\text{A}$	Vbr	V	4.5	7	-
SSB Noise Figure	NF	dB	-	6.5^4	-

Table 11.1: Datasheet for the M/A-Com MA4E1317 Schottky diode [21].

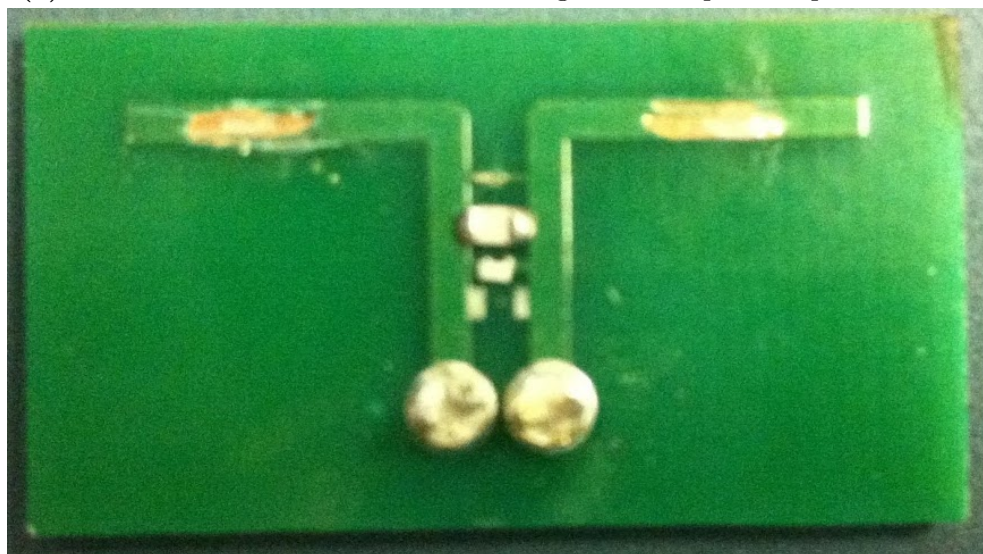
11.3 Antenna Design

A printed circuit board (PCB) half-wave dipole was chosen as the antenna for the system. The copper trace acts as the antenna, and is etched into a FR-4 substrate. The MA4E1317 is a flip-chip device, and is only suitable for mounting on a PCB. The design and specific parameters of the antenna is based off of the dual frequency WPT rectenna in [29], but has been modified in our implementation. The design of the rectenna is shown in Figure 11-1.

The rectenna is composed of the MA4E1317 diode, a 47 pF ceramic capacitor acting as a low-pass microwave filter, a $330\ \Omega$ load resistor, and output pins for measurement purposes. The antenna is designed for operation at 5.45 GHz, so the length of the dipole is 27.55 mm, half the wavelength of the incident wave.



(a) A schematic of the PCB rectenna design and component specifications.



(b) Image of the assembled rectenna

Figure 11-1: Rectenna design

One important distinction for this rectenna design is the lack of filtering for higher-order harmonics. This feature is common in most rectennas, but is deliberately left out so that the antenna can generate nonlinear harmonics from the interrogation signal.

No special consideration for impedance matching between the antenna and the rectifier components. This is definitely a point to consider for future improvement,

as proper matching of the components should significantly improve the efficiency of rectification.

11.4 Rectenna Testing

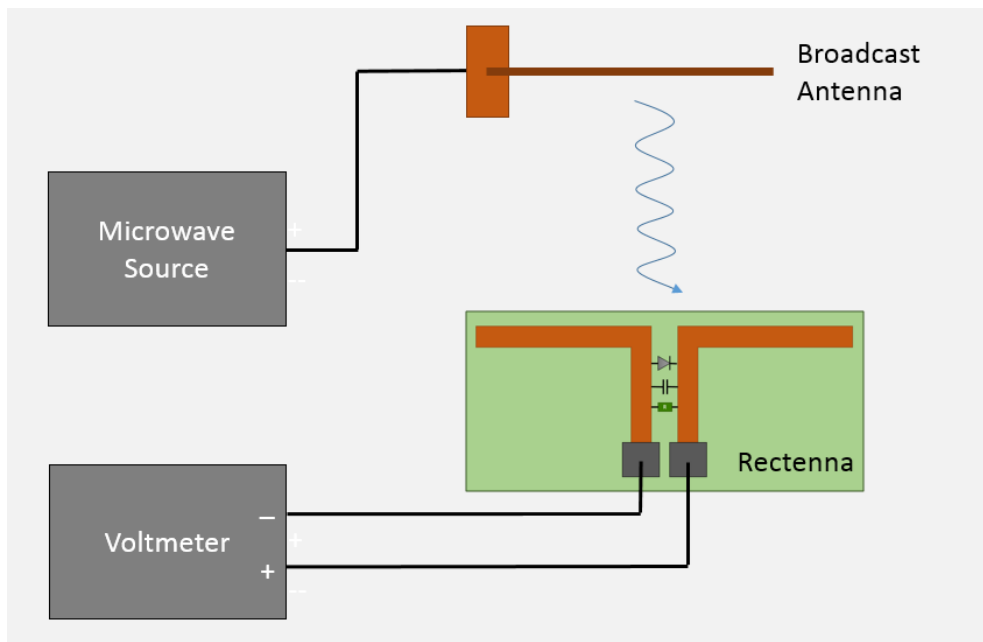
To thoroughly test the rectenna, distinct tests were run to order to verify both its rectification and harmonic generation capabilities. We examined a range of frequencies for all tests to isolate peak performance.

11.4.1 DC Power Characterization

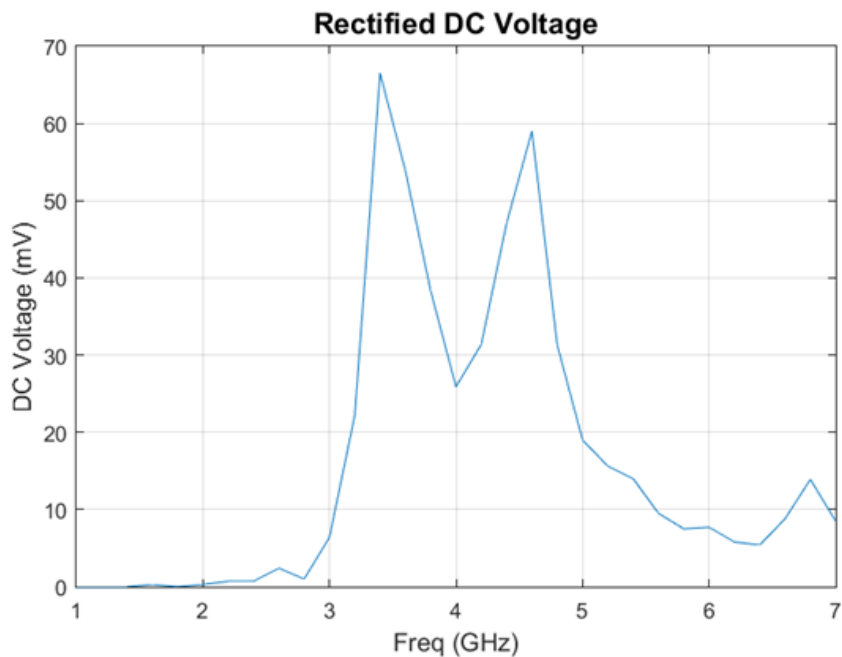
To determine the overall rectification efficiency, a second antenna was used to broadcast energy to the rectenna. A 17 dBm CW signal was generated from the PSG and broadcast through a monopole antenna. The rectenna was then positioned parallel to the broadcast antenna, at a distance of 2 cm. and the average DC voltage and power was measured over the load resistor. The test was repeated over a range of broadcast frequencies from 1 to 7 GHz. The setup is shown in Figure 11-2a and the results are shown in Figure 11-2b.

Rectification was most pronounced in the 3-5 GHz frequency band. Rectified voltage is highest at 3.4 GHz and 4.6 GHz, with DC voltage levels of 66.5 mV and 59.0 mV respectively. Unfortunately, DC voltage results of higher frequencies were unreliable and erratic given the measurement techniques, and accurate data could not be taken.

Given the resistive load of 330Ω , rectified DC power can be calculated from the



(a) Experimental setup for rectification testing



(b) DC voltage measured from the voltmeter in the setup on the left for a range (1-7 GHz) of frequency inputs.

voltage above. Using DC voltage (V) and load resistance (R), the DC power (P_{dc})

was calculated using Equation 11.1:

$$P_{dc} = \frac{V^2}{R} \quad (11.1)$$

A plot of this is shown in Figure 11-3.

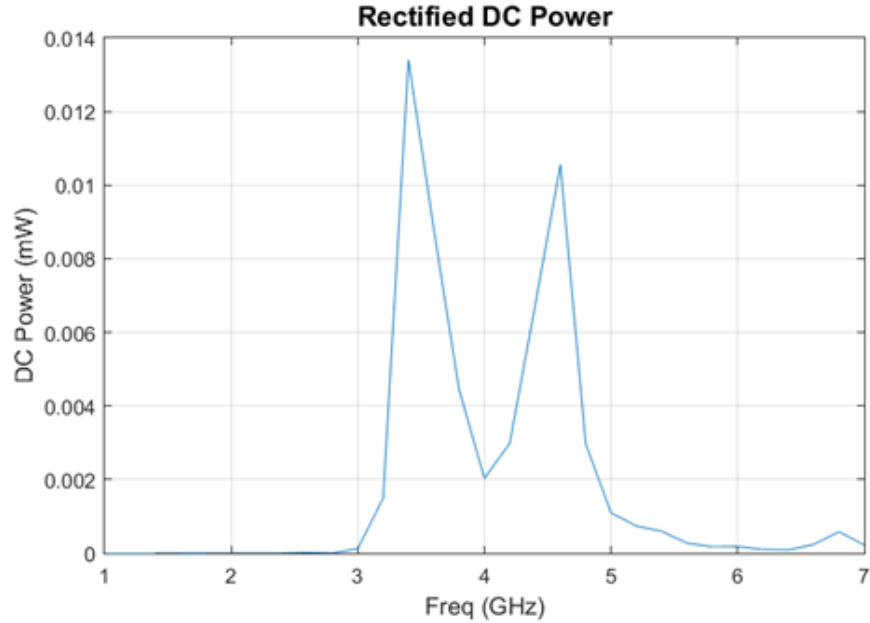


Figure 11-3: Rectified DC power calculated from DC voltage using the relation:
 $P = \frac{V^2}{R}$

Considering the input power of 17 dBm (around 50.12 mW), the wall-to-load efficiency of the experiment is extremely low for all frequencies. These losses can come from a number of sources, including bad coupling between the broadcast antenna and rectenna, reflection from broadcast antenna, losses in coaxial connections between components, and power radiated away from the rectenna, among others. However, the inherent losses of the experimental setup are not relevant to the overall efficiency of the system; for this, the efficiency result must be compared to only the rectification efficiency.

To establish rectification efficiency, AC power tests were conducted on a bare dipole antenna with no diode, resistor, or capacitor. The results of this test establish the overall power accepted by the rectenna, and is directly comparable to the previous DC power results.

The setup of the AC power experiment was similar to the DC power experiment, with the exception of two key differences: the voltmeter was replaced by a DS091304A oscilloscope, and the rectenna was replaced by the bare dipole antenna. In the absence of the $330\ \Omega$ load resistor on the rectenna, the $50\ \Omega$ input impedance of the oscilloscope [20] was used as the load.

Using AC voltage amplitude (V_{max}) and load resistance (R), the accepted AC power (P_{ac}) was calculated using Equation 11.2:

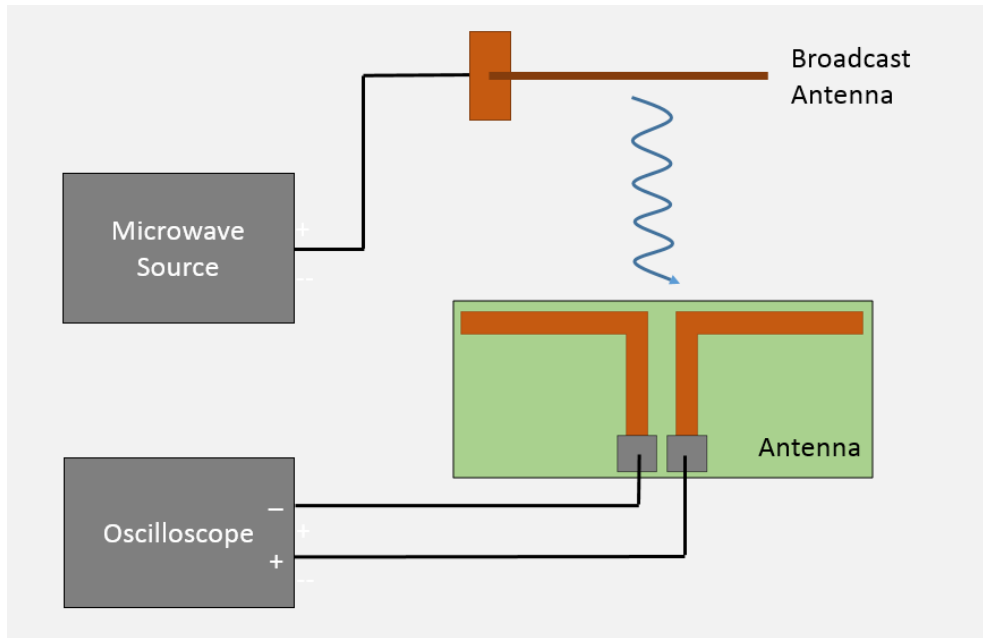
$$P_{ac} = \frac{V_{max}^2}{2R} \quad (11.2)$$

The setup and results of the test are shown below in Figures 11-4a and 11-4b, respectively.

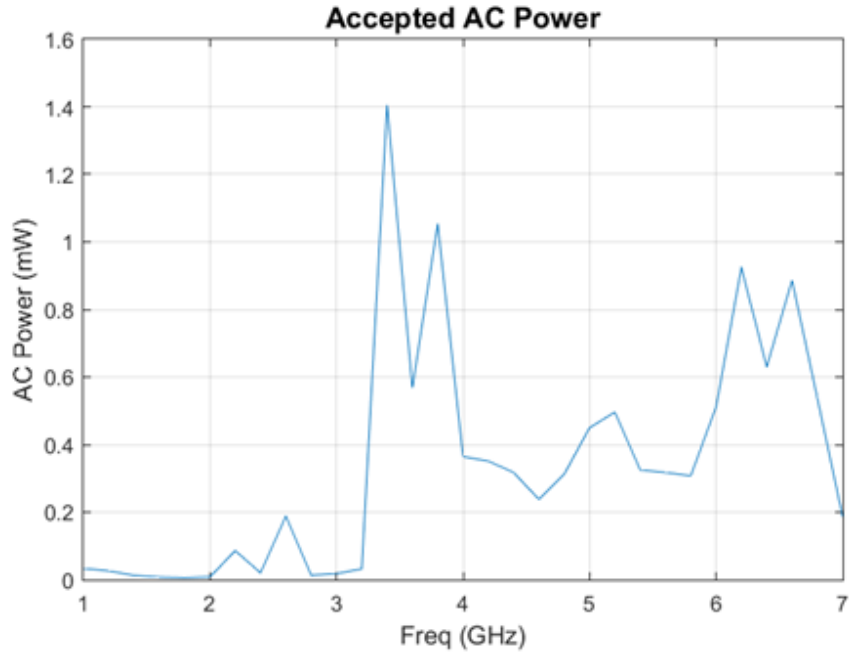
Assuming that the transfer function between the antennas doesn't change between the AC and DC tests, these results allow the rectification efficiency to be calculated. The efficiency (E) in this case is the ratio of the rectified DC power (P_{dc}) to the total accepted AC power (P_{ac}), as in Equation 11.3:

$$E = \frac{P_{dc}}{P_{ac}} \quad (11.3)$$

Figure 11-5 shows the efficiency calculated this way, across the range of frequencies



(a) Experimental setup for measuring accepted AC power



(b) Accepted AC power, used to establish a baseline for efficiency calculation, calculated using the relation $P = \frac{V_{max}^2}{2R}$.

tested.

Analysis of the graph shows the same peak rectification efficiencies at 3.2 GHz and 4.6 GHz, with 4.7% and 4.4% respectively. This rather low efficiency is expected

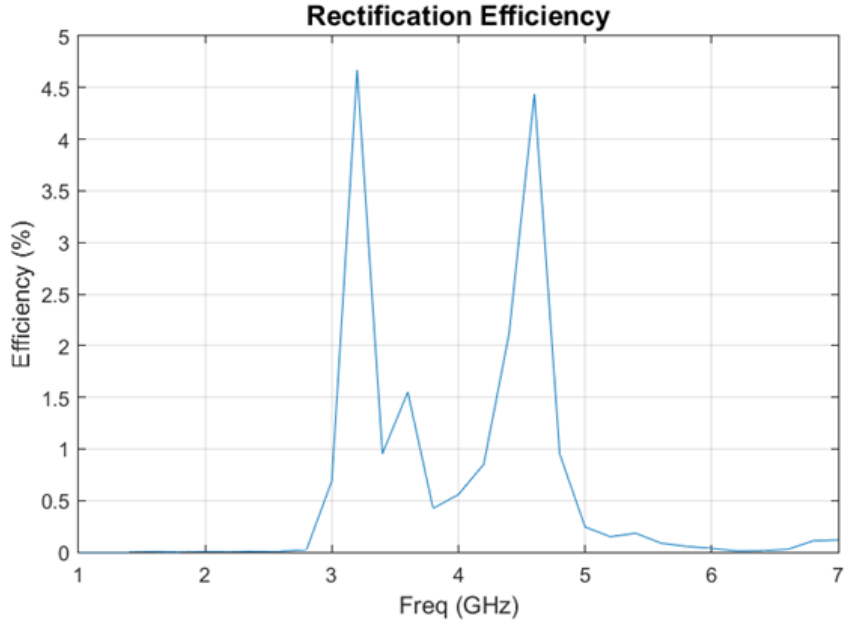


Figure 11-5: Rectification efficiency, calculated using accepted AC power as a baseline. Calculated using the ratio of rectified DC power to accepted AC power.

given the lack of optimization and impedance matching in the rectenna. However, this result clearly demonstrates rectification of high frequency AC power.

11.4.2 Harmonic Generation

Harmonic generation was then tested by measuring second harmonic power reflected from the rectenna. The antenna was stimulated by a 0 dBm CW signal, and the second harmonic reflected from the antenna was collected using a directional coupler feeding into the spectrum analyzer for measurement. The test setup for and results are shown in Figure 11-6.

In initial testing, the harmonic generation of the rectenna was minimal, as the measured 2nd harmonic power was comparable to the noise level power. However, after filtering out harmonic responses from microwave source, a distinct 2nd harmonic

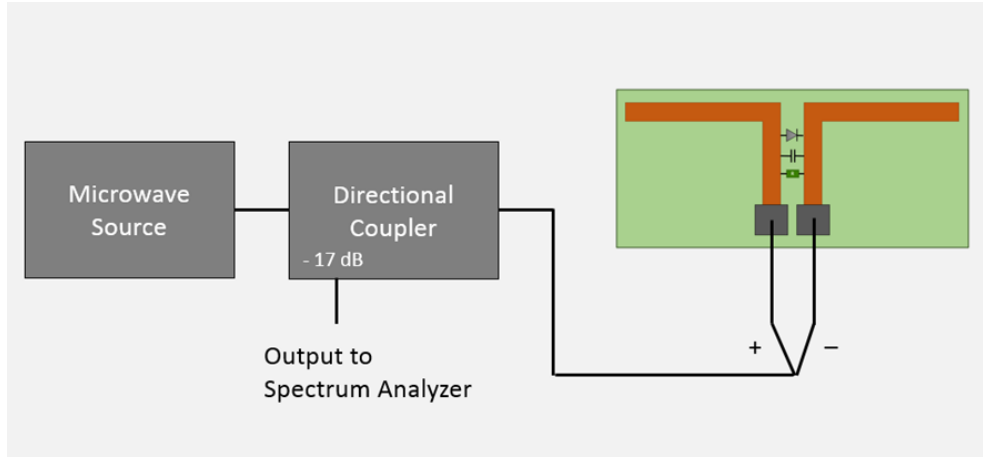


Figure 11-6: Experimental setup for harmonic generation testing.

was found at 2.45 GHz at -150 dBm compared to the noise level power of -161 dBm. Bandwidth restrictions of filtering components prevented analysis of a full frequency spectrum, and thus, 2.45 GHz is the only frequency we were able to probe for harmonics. Even so, this result does demonstrate the harmonic generation capabilities of the rectenna.

11.5 Discussion

The intent of the rectenna was twofold. The rectenna was designed to rectify RF signals (1–10 GHz) and generate of higher-order harmonics. Both of these qualities are needed for the creation of an NLTR rectifier. The current experiments establish a baseline for rectification and harmonic generation that can be used for future designs.

The current design has made no steps towards the impedance matching of the antenna to the components. This is likely a major source of power lost by the system for rectification, and should be a top priority to consider in subsequent designs.

Our design of a dual-purpose rectenna satisfied our initial goals, and is a first step

towards a functioning NLTR based WPT system. After considerable optimization and miniaturization, the rectenna would be used as a receiver for the electronics we want to power. After receiving the initial interrogation pulse and generating the 2nd harmonic response, it would then receive the main high power pulse and rectify the signal, providing the load device with DC power. Due to the nature of NLTR, the receiving devices do not require power to facilitate the process.

Chapter 12

Conclusion

In summary, here is a review of our collected investigations.

12.0.1 Equipment and Expertise Limitations

Concerning spatial profiling experiments, the trials conducted by TESLA suggest that the region of excitation around a target could be relatively broad compared to the size of our antenna. Following this, the team wanted to see whether it was possible to take advantage of this result through repeated re-targeting of an antenna while it moved away from the region of greater power. It was hoped that a positive result would confirm that a TR WPT system could maintain steady power delivery to a moving target. Our results appear suggest that it should be, though TESLA was somewhat limited by the time our TRM took to aquire a new sona and retarget the antenna.

TESLA's research also investigated how antenna design and form could relate to TR convergence. This path yielded inconclusive results for a variety of reasons. Due

to lack of resources and relative inexperience, the team approached antenna design and testing using a “rapid prototyping” plan that resulted in inconsistent designs. Higher quality fabrication techniques, coupled with prototypes in computer simulations, could have improved this aspect of research. We suggest that future research in TR antenna optimization focus on the creation of nonlinearly reflective antennas useful in NLTR with consistent quality. These antennas will allow experiments on TR WPT with multiple receivers, a topic which may offer significant advances in the field.

To better investigate TR’s applicability to WPT, the team attempted to map how broad and how strong the excitation a collapsing wavefront was around a target antenna. An understanding of this would be useful to future engineers attempting to integrate a TR WPT system into any larger system. Reconstruction were mapped at a variety of frequencies, and the width of this spatial profile was found to be directly related to the wavelength.

On the topic of overlapping sonas, we hypothesized that overlapping reconstructions could result in more effective power transmitted per duty cycle. Our experiments seemed to support this, with an increased number of reconstructions per cycle continuing to maintain their characteristic shape. However, one setback in our experimentation was the Agilent E8267D Vector PSG, which attempted to scale each arbitrary waveform broadcast to the same total output power. This prevented us from definitively concluding a relationship between the number of reconstructions and the power received by the target.

Better tools can also help the team revisit previously unsuccessful experiments. The

team investigated whether ferromagnetic nanorods could be used to produce a distinctive nonlinear signature, but these tests were inconclusive. TESLA could not identify the presence of a strong nonlinear signal at the scanned frequencies, though a different setup or frequency range may yield more conclusive results.

As discussed in the literature review, prior research has distinguished between linear and nonlinear elements. We wanted to demonstrate that it was also possible to distinguish between two distinct nonlinear elements. While we were successful in replicating previous work distinguishing linear and nonlinear elements, we were not able to produce two nonlinear elements that were sufficiently different and identifiable in their nonlinear response in frequency domain. However, we remain convinced that this is possible based on the results of our simulations.

Additionally, we attempted to make our own rectenna that would both rectify incoming microwaves to a DC voltage and act as a nonlinear element for NLTR. We were able to demonstrate both these capabilities in a test environment. However, significant optimization remains necessary before our rectenna is usable for full-scale NLTR-based WPT.

12.0.2 Future Work and Considerations

TESLA's research into TR was very much a learning experience. The team began its research with little to no experience with TR. As a result, many of the team's early research results should be reconsidered or revisited. There are other areas that the team did not investigate at all, and which now are obvious areas of research.

TESLA’s experimentation focused significantly on the relationship between sona and reconstruction, and there are more areas within this topic that should be revisited in greater detail. TESLA performed several early experiments on partial sonas to see how they relate to reconstruction quality. However, the team prioritized completion of other tests at the time, as there was an unclear sense of practical application or benefit by continuing. In retrospect, these tests may be useful in relating the sona to the environmental characteristics and should be considered in more detail.

Future researchers may want to consider the quality of reconstructions created with partial sonas. This research should also give a better quantification of what “reconstruction quality” means for arbitrary reconstruction waveforms. It could be beneficial to find methods of relating sona length and general shape to geometric factors of the environment. Understanding this relationship can allow the optimization of a TR WPT system for a given environment. The reverse is also true; some modifications to the transmission environment may help improve efficiency.

Finally, the effect of iterative time reversal on reconstruction was ignored in TESLA’s tests. The team suggests that it should be considered in future experimentation. Iterative time reversal mirrors are common in the literature for signal focusing, and there is reason to believe that iteration will also improve EM TR WPT. Iteration may have significant effects on transfer efficiency and spatial profile. However, iteration is also based off of the idea of a stationary target, and may not work well for moving targets. This tradeoff, once understood, will greatly help optimize the system.

The aluminum echoic chamber used in tests (the Gigabox), and the equipment

used to transmit and measure EM waves within this chamber were from previous experiments on TR done by graduate students under Dr. Anlage. These resources allowed TESLA a great deal of freedom in designing and conducting experiments. However, monetary and physical resources of the team limited the purchase of additional equipment, which in turn restricted the experiments that could be done.

The Gigabox was designed to be an ideal environment to study TR from a signal processing point of view. However, the Gigabox is not easily modifiable. A Gigabox with interchangeable panels will allow for the creation of testing environments of differing absorption, translucence, and geometry. Finer control of these parameters will aid the development of a model for the effects of environment on the power losses of TR WPT. The lack of this model for transmission efficiency is one of the greatest challenges towards designing a TR WPT system.

Thanks to the generosity of Dr. Anlage and the UMD CNAM, Team TESLA had access to several state-of-the-art measuring and testing devices. Researching alongside graduate students associated with the CNAM, TESLA explored TR WPT primarily through the behavior of reconstruction, including how sonas can be manipulated to change reconstruction parameters. Experiments including minimum TR cycle time, overlapping sonas, and reconstruction profile characterization have added to the literature surrounding practical TR, but gaps in knowledge continue to remain. Many of these gaps we have identified are due to limitations in TESLA's technical expertise and lack of access to proper equipment. As a result of these shortcomings, we suggest areas of further research that could yield fruitful results with a dedicated and pioneering team, including what experiments could address these gaps. It is our

hope that our research will lay groundwork for further explorations of how TR can be applied to practical WPT.

Glossary

active transmission A WPT system where both transmitter and receiver expend some power to maintain the process.

anisotropic scatterer A scattering element with a directional bias.

AWG Arbitrary Waveform Generator.

carrier frequency The frequency of the carrier wave for our interrogation process..

CNAM Center for Nanophysics and Advanced Materials.

collapse The movement of a time reversed sona towards its point of convergence. The collapse occurs as the reflections of the sona interfere constructively at the point of convergence.

CST Computer Simulation Technology: Microwave Studio.

DORT Decomposition of the Time Reversal Operator.

DSO Digital Storage Oscilloscope.

efficiency The ratio of usable energy delivered to the total energy broadcast by a WPT system. How efficiency is measured can vary wildly based on methodology. In this paper we will define efficiency as being the total power delivered to a load, compared to the total power drawn by the transmitter.

EM Electromagnetic.

FDTD Finite Difference Time Domain.

FFT Fast Fourier Transform.

FIT Finite Integration Technique.

Gigabox The microwave cavity used for our experimental TRM.

HRMC Highly Resonant Magnetic Coupling.

impedance matching Adapting the impedance of a load to the impedance of a power source, such that power delivered to the load is maximized.

injecting port A port designated for broadcasting (injecting) signals. The transmitter of the TRM.

interrogation pulse The signal injected into the cavity at the transmitter in order to obtain a sona.

knee voltage The voltage necessary for “turning on” a diode.

linear time reversal Time reversal involving a transmitter and receiver. Requires some separate method of communication of sonas between transmitter and receiver.

LTR Linear Time Reversal.

maximum power The maximum amount of power that can be transmitted to a target using a given wireless power transfer system.

mode An eigenfunction of the wave equation given the boundary conditions of a system.

mode density A description of the separation of modes in terms of frequency (energy) separation; as $\delta f = 0$ the mode spectrum tends to form a continuum.

NLTR Nonlinear Time Reversal.

nonlinear time reversal Time reversal involving a transmitter and nonlinear receiver. During use the nonlinear receiver will generate nonlinear harmonics allowing the sona that it generates to be filtered out from background noise.

parasitic capacitance The unwanted capacitance introduced from the arrangement of components in an electrical network along with materials.

passive transmission A WPT system where only the transmitter expends power to maintain the process.

port An hole on the Gigabox, used to transmit signals into the Gigabox, and record signals within it.

PSG Pulse Signal Generator.

pulse inversion The signal processing technique for isolating the nonlinear component of a signal.

PWM Pulse Width Modulation.

range The maximum distance that a wireless power transfer system can transmit a given amount of power.

ray chaotic environment An important feature of a chaotic system where there is a sensitive dependence on initial conditions; if one were to consider two ray originating at a given point with an arbitrarily small angle in separation, the forward ray traces quickly diverge. For our application, the implication is these ray traces will cover the volume of the cavity.

receiver The component of a WPT system that has a net input of power into the system.

reconstruction A focused signal produced as the result of a TR process. Reconstructions are formed from the injection of time-reversed sona at the transmitter.

recording port A port designated for recording broadcasts injected into the cavity. The receiver of the TRM.

rectenna A rectifying antenna. It collects electromagnetic power and converts it into usable DC power. This device is commonly used in wireless power transfer systems.

RF Radio Frequency.

S parameters The parameters of a scattering matrix which describe a linear electronic networks's transmission/reflection of an approaching EM wave.

scatterer An element that functions to isotropically scatter ambient waves. A reflector.

short-orbit The mechanism responsible for the multiple reconstruction signals appearing at different time intervals.

sona Sona: originating from sonabilis, resonant. The signal recovered at the receiver during the interrogation stage of a TR process. During a TR process the sona is time reversed and injected into the cavity to form a reconstruction at a receiver.

time reversal Time reversal can refer to (1) the property of time reversal symmetry in the system; or (2) the signal focusing technique using said property.

TR Time Reversal.

transmitter The component of a WPT system that outputs power into the system.

TRM Time Reversal Mirror.

TRR Reverse Recovery Time.

WPT Wireless Power Transfer.

Bibliography

- [1] First GSM-based communicator product hits the market Nokia Starts Sales of the Nokia 9000 Communicator, August 1996.
- [2] A brief history of Wi-Fi. *The Economist*, June 2004.
- [3] W Ross Adey. Biological effects of electromagnetic fields. *Journal of cellular biochemistry*, 51(4):410–416, 1993.
- [4] APD Semiconductor. *AN-1012: Reverse Recovery Time (TRR) of the Super Barrier Rectifier*, 2006.
- [5] Galen Carol Audio. Decibel(loudness) comparison chart. Retrieved from website: <http://www.gcaudio.com/resources/howtos/loudness.html>, aug 207.
- [6] E. Barbieri and M. Meo. Time reversal DORT method applied to nonlinear elastic wave scattering. *Wave Motion*, 47(7):452–467, November 2010.
- [7] Kenneth Butler. Tour WiTricity’s Room of Tomorrow: Wireless Charging That’s Flexible, December 2013.
- [8] D. H. Chambers. Target characterization using time-reversal symmetry of wave propagation. *International Journal of Modern Physics B*, 21(20):3511–3555, August 2007.
- [9] Roger Cheng. Ikea to sell furniture that can wirelessly charge your phone. Retrieved from website: <http://www.cnet.com/news/ikea-to-sell-furniture-that-can-wirelessly-charge-your-phone/>, feb 205.
- [10] Josh Constine. uBeam Declassifies Secrets To Try To Prove Wireless Power Is Possible, November 2015.
- [11] Energous Corporation. Product overview. Retrieved from website: <http://www.energous.com/product-overview/>, aug 2016.
- [12] Sam Davis. Schottky diodes: the old ones are good, the new ones are better. *Power Electronics*, 2011.
- [13] Mathias Fink and others. Time-reversed acoustics. *Scientific American*, 281(5):91–97, 1999.

- [14] Matthew Frazier, Biniyam Taddese, Thomas Antonsen, and Steven M Anlage. Nonlinear time reversal in a wave chaotic system. *Physical review letters*, 110(6):063902, 2013.
- [15] Matthew Frazier, Biniyam Taddese, Bo Xiao, Thomas Antonsen, Edward Ott, and Steven M Anlage. Nonlinear time reversal of classical waves: Experiment and model. *Physical Review E*, 88(6):062910, 2013.
- [16] Griffiths, David. *Introduction to Electrodynamics*. Prentice Hall, 3 edition, 1999.
- [17] Sameer Hemmady, Xing Zheng, James Hart, Thomas M Antonsen Jr, Edward Ott, and Steven M Anlage. Universal properties of two-port scattering, impedance, and admittance matrices of wave-chaotic systems. *Physical Review E*, 74(3):036213, 2006.
- [18] Sun K. Hong, Victor M. Mendez, Trystan Koch, Walter S. Wall, and Steven M. Anlage. Nonlinear Electromagnetic Time Reversal in an Open Semireverberant System. *Physical Review Applied*, 2(4), October 2014.
- [19] Morris Kesler. Highly Resonant Wireless Power Transfer: Safe Efficient and over Distance. Technical report, WiTricity, Watertown MA, 2013.
- [20] Keysight Technologies. *Infinium 90000 Series Oscilloscopes*. Rev. V8.
- [21] Macom. *GaAs Flip Chip Schottky Barrier Diodes*. Rev. V8.
- [22] Dinh-Quy Nguyen and Woon-Seng Gan. The DORT solution in acoustic inverse scattering problem of a small elastic scatterer. *Ultrasonics*, 50(8):829–840, August 2010.
- [23] C. Prada. The iterative time reversal mirror: A solution to self-focusing in the pulse echo mode. *The Journal of the Acoustical Society of America*, 90(2):1119, 1991.
- [24] Claire Prada, SÃ©bastien Manneville, Dimitri Spoliansky, and Mathias Fink. Decomposition of the time reversal operator: Detection and selective focusing on two scatterers. *The Journal of the Acoustical Society of America*, 99:2067, 1996.
- [25] ProCon. 20 highest and lowest radiation cell phones. Retrieved from the CST website <http://cellphones.procon.org/view.resource.php?resourceID=003054>, aug 2015.
- [26] John B Schneider. Understanding the finite-difference time-domain method. *School of electrical engineering and computer science Washington State University.–URL: http://www. Eecs. Wsu/ ~ schneidj/ufdtd/(request data: 29.11. 2012)*, 2010.

- [27] David Hope Simpson, Chien Ting Chin, and Peter N. Burns. Pulse inversion Doppler: a new method for detecting nonlinear echoes from microbubble contrast agents. *Ultrasonics, Ferroelectrics, and Frequency Control, IEEE Transactions on*, 46(2):372–382, 1999.
- [28] Walter Fox Smith. *Waves and oscillations: a prelude to quantum mechanics*. Oxford University Press, New York, 2010.
- [29] Young-Ho Suh and Kai Chang. A high-efficiency dual-frequency rectenna for 2.45-and 5.8-ghz wireless power transmission. *Microwave Theory and Techniques, IEEE Transactions on*, 50(7):1784–1789, 2002.
- [30] Binyam Tesfaye Taddese, Thomas M. Antonsen, Edward Ott, and Steven M. Anlage. Sensing small changes in a wave chaotic scattering system. *Journal of Applied Physics*, 108(11):114911, 2010.
- [31] Computer Simulation Technology. The finite integration technique. Retrieved from the CST website <https://www.cst.com/Products/CSTMws/FIT>.
- [32] C.A. Tucker, K. Warwick, and W. Holderbaum. A contribution to the wireless transmission of power. *International Journal of Electrical Power & Energy Systems*, 47:235–242, May 2013.
- [33] Beibei Wang, Yongle Wu, Feng Han, Yu-Han Yang, and K. J. Ray Liu. Green Wireless Communications: A Time-Reversal Paradigm. *IEEE Journal on Selected Areas in Communications*, 29(8):1698–1710, September 2011.
- [34] M Clemens T Weiland. Discrete electromagnetism with the finite integration technique. *Progress In Electromagnetics Research*, 32:65–87, 2001.
- [35] Wi-Charge. How it works. Retrieved from website: <http://www.wi-charge.com/technology.php?ID=25>, mar 2016.